Understanding Boreal Summer UTLS Water Vapor Variations in Monsoon Regions: A Lagrangian Perspective

Hongyue Wang¹, Mijeong Park², Mengchu Tao³, Cristina Peña-Ortiz⁴, Nuria Pilar Plaza⁵, Felix Ploeger^{1,6}, and Paul Konopka¹

Correspondence: Paul Konopka (p.konopka@fz-juelich.de)

Abstract. Water vapor in the upper troposphere and lower stratosphere plays a crucial role in elimatefeedbackfor climate, affecting radiation, chemistry, and atmospheric dynamics. This study presents applies simplified Lagrangian reconstructions of stratospheric water vapor satellite observations from SAGE from SAGE III/ISS and MLS instruments, to improve the understanding of moist anomalies satellite observations, in order to improve understanding of moisture enhancements in the Asian and North American monsoons and to identify the key factors contributing to model biases. Our findings show that while both SAGE III/ISS and MLS satellite datasets capture similar spatial patterns, SAGE III/ISS shows higher local values. The performance of Lagrangian reconstructions significantly improves with the size of trajectory ensembles but exhibits a general dry biasacross the tropics. However, the. The reconstruction represents the Asian monsoon moist anomaly well-summertime local water vapor maximum well in the Asian monsoon, particularly above the tropopause, whereas it fails to capture but not in the North American monsoonanomaly. The main dehydration, region as region diagnosed from trajectories, indicates that water vapor in the Asian monsoon is predominantly controlled by local temperatures near the tropopause in the Asian Monsoon. tropopause temperatures. The dry bias in reconstructions below the tropopause over the Asian monsoon shows a positive correlation with convection intensity, particularly in the western part of the monsoon region, suggesting that underestimated moistening from convection may contribute to this bias. Water vapor mixing ratios in the North American monsoon is are largely influenced by long-range transport from dehydrated regions over Southeast Asia, while moist air masses are primarily controlled by local dehydration. Hence, the southern Asia and additional local moistening. The limited performance of the reconstruction for reconstructions in the North American monsoon is potentially linked to an therefore likely linked to underestimation of local convection or uncertainty uncertainties in long-range transport. Additionally, dry bias in reconstruction over the Asian monsoon shows a positive correlation with intensity of convection particularly in the western sector, suggesting that an underestimation of moistening due to convective ice injection may play a role in this region.

¹Institute of Climate and Energy Systems, Stratosphere (ICE-4), Forschungszentrum Jülich, 52428 Jülich, Germany

²U.S. National Science Foundation National Center for Atmospheric Research (NSF NCAR), Boulder, CO 80307, USA

³Carbon Neutrality Research Center, Institute of Atmospheric Physics, Chinese Academy of Sciences, Beijing 100029, China

⁴Departamento de Sistemas Físicos, Químicos y Naturales, Universidad Pablo de Olavide, 41013 Seville, Spain

⁵Centro de Investigaciones sobre Desertificación, Consejo Superior de Investigaciones Científicas (CIDE-CSIC), 46113 Moncada, Valencia, Spain

⁶Institute for Atmospheric and Environmental Research, University of Wuppertal, 42119 Wuppertal, Germany

1 Introduction

Stratospheric water vapor (H₂O) is a potent greenhouse gas that can significantly amplify warming of the global temperature global warming due to its strong radiative effects and long residence time (Solomon et al., 2010; Riese et al., 2012). The amount of water vapor entering the stratosphere is primarily controlled largely determined by the freeze-drying process—the dehydration of moist tropospheric air as it ascends while ascending through the cold point tropospheric air as it ascends while ascending through the cold point tropospheric air as it ascends while ascending through the cold point tropospheric air as it ascends while ascending through the cold point tropospheric air as it ascends while ascending through the cold point tropospheric air as it ascends as it ascends as it ascends as it as it ascending through the cold point tropospheric air as it ascends as it as i 1949; Randel and Park, 2019; Smith et al., 2021). This freeze-drying process occurs mainly in the tropical tropopause layer (Fueglistaler et al., 2009), where air masses ascend slowly (diabatically) from the level of main convective outflow undergo slow diabatic ascent into the stratosphere over timescales of weeks to months. During this ascend, air parcels travel horizontally over ascend, the air masses travel thousands of kilometers and likely in the horizontal direction and often sample the coldest tropopause regions (the 'cold trap') (Holton and Gettelman, 2001). On the other hand, water vapor and ice can be directly injected into the Upper Troposphere and Lower Stratosphere (UTLS) through by deep, overshooting convection, and it has been argued that this process happens and related strong vertical updrafts near the convective centers on timescales of minutes (Jorgensen and Lemone, 1989; Schwartz et al., 2013). Such convection-driven transport has been reported to occur frequently in the tropics and over North America during boreal summer (Homeyer et al., 2023). This convection-driven transport is characterized by rapid vertical updrafts near convective centers, occurring in the timescales on the order of minutes (Jorgensen and Lemone, 1989; Schwartz et al., 2013). However, the extent to which this hydration process affects stratospheric water vapor remains under debate (Randel et al., 2012; Avery et al., 2017; Uevama et al., 2020; Jensen et al., 2020; Uevama et al., 2023; Homeyer et al., 2023; Konopka et al., 2023).

During boreal summer, enhanced water vapor is observed in the UTLS over regions influenced by the Asian Summer

Monsoon (ASM) and North American Monsoon (NAM) (Ploeger et al., 2013; Park et al., 2021; Clemens et al., 2022). This
enhancement is often regions exhibits enhanced water vapor mixing ratios (Ploeger et al., 2013; Park et al., 2021; Clemens et al., 2022)
. This water vapor enhancement is strongly associated with seasonal variations in tropical tropopause temperatures and circulation
(James et al., 2008; Uma et al., 2014) and is also attributed to intense convection, which that can transport water vapor directly into the UTLS (Fu et al., 2006; Yu et al., 2000) (Fu et al., 2006; Yu et al., 2020). Besides localized convection, seasonal
variations in tropical tropopause temperatures play a key role in modulating UTLS water vapor levels, with peak concentrations
occurring in boreal summer and autumn (Randel et al., 2004; Tao et al., 2023). In particular, the ASM has been recognized as
a major contributor to stratospheric water vapor, accounting for -15% of the tropical stratospheric water vapor anomaly and
-30% of the summertime NH extratropical water vapor maximum (Bannister et al., 2004; ?; Rolf et al., 2018; Nützel et al., 2019)
. These observational studies, however, have limitations in understanding the physical processes that are driving the enhancement
in water vapor concentrations over the monsoon regions. Understanding those mechanisms and the interactions between
However, a detailed understanding of the mechanisms and interactions among regional convection, large-scale transport, and
thermodynamic conditions is the key to predict the potential impact of in the monsoons and their effects on stratospheric water
vapor on our elimate, has not been achieved, but is crucial for assessing related climate impacts.

In this study, our goal is to evaluate the role of the freeze-drying mechanism in the large-scale temperature and wind
fields for the enhancement of stratospheric water vapor over the ASM and NAM regions from a Lagrangian perspective The
advection-condensation paradigm (Pierrehumbert and Roca, 1998; Liu et al., 2010) describes atmospheric water vapor distributions
as being primarily controlled by advection through the saturation mixing ratio field. Lagrangian methods track the history of air
parcels (their trajectories) and reconstruct stratospheric water vapor based on the coldest temperature encountered along these
trajectories, commonly referred to as the simulate the motion of air masses and quantify the dehydration process by identifying
the coldest temperatures encountered along troposphere-to-stratosphere trajectories (TST). These coldest points, termed Lagrangian cold points (LCP) temperature (Fueglistaler et al., 2005). By capturing the cumulative effects of large-scale transport
and temperature variability over timescales ranging from days to months, Lagrangian LCPs) (Fueglistaler et al., 2005), provide
the essential diagnostic for applying the advection-condensation paradigm to stratospheric dehydration. Such methods have
been successfully used to reproduce UTLS widely applied to reproduce regional and temporal water vapor anomalies in the

UTLS (Mote et al., 1995; Fueglistaler and Haynes, 2005; Liu et al., 2010; Schoeberl and Dessler, 2011; Smith et al., 2021).

We firstly conduct Lagrangian back-trajectory simulations utilizing the trajectory module of the Chemical Lagrangian Model
of the Stratosphere (CLaMS) (McKenna et al., 2002), to reconstruct satellite observations by

Here, we aim at evaluating dehydration processes in the UTLS over the ASM and NAM regions from a Lagrangian perspective. The main research questions explored in this paper are:

- How well can UTLS water vapor mixing ratios in the ASM and NAM be reconstructed using a simplified Lagrangian modelling method, especially in comparison to the tropics?
 - Are the moisture enhancements observed within the ASM and NAM anticyclones locally or remotely controlled and which regions contribute most strongly to these enhancements?
 - Are model biases in the reconstruction related to particular processes (e.g., convection)?
- Station (SAGE III/ISS) Davis et al. (2021) Version 5.3 and which have relatively high vertical resolution compared to other satellite observations. In addition, we use observations from the Aura Microwave Limb Sounder (MLS) Version 5.0 Lambert et al. (2017). These Lagrangian reconstructions are—which provide daily global coverage and have been widely used in studies of stratospheric water vapor (Mote et al., 1995; Liu et al., 2010; Nützel et al., 2019). To reconstruct the satellite observations, we perform Lagrangian backward trajectory simulations with the trajectory module of the Chemical Lagrangian Model of the Stratosphere (CLaMS), driven by the fifth generation European Centre for Medium-Range Weather Forecasts atmospheric reanalysis (ERA5)(Hersbach et al., 2020). We then assess the performance of the Lagrangian reconstruction in capturing boreal summer—The reconstruction performance in capturing UTLS water vapor distributions by comparing simulation results to is evaluated by comparison with the satellite observations. Additionally, we compare and by contrasting the monsoon regions to the deep with the tropics, where similar Lagrangian reconstructions were methods have been successfully applied in the past (Fueglistaler et al., 2005; Hasebe and Noguchi, 2016; Smith et al., 2021). SAGE III/ISS is utilized for its higher

vertical resolution (2 km compared to ~3 km in MLS near the UTLS region (Read et al., 2007)), providing a more detailed representation of water vapor vertical structures within the monsoon anticyclones. In addition, MLS provides daily global coverage and has widely been used in numerous studies on stratospheric water vapor Mote et al. (1995); Liu et al. (2010); Nützel et al. (2010). Furthermore, we analyze the spatial and temporal locations of the LCPs in relation to observed water vapor distributions within the monsoon regions. We also investigate the potential Finally, we determine the dehydration regions and investigate factors contributing to discrepancies between the Lagrangian differences between reconstructions and observations, with a particular focus on deep convection, which is only partly resolved in ERA5 meteorology. As a proxy for the intensity of convection, we use Outgoing Longwave Radiation (OLR) derived from satellite observations (Kumar and Krishnan, 2005).

The main research questions explored in this paper are: (i) How well can stratospheric water vapor mixing ratios in the ASM and NAM as observed by SAGE III/ISS and MLS be reconstructed using a simplified Lagrangian modelling method, especially in comparison to the deep tropics? (ii) Are the moisture anomalies observed within the ASM and NAM anticyclones locally or remotely controlled by the LCPs and which regions are most critical? (iii) Are model biases in the reconstruction related to particular processes (e.g., convection)?

the role of deep convection.

This paper is organized as follows: Section 2 presents the datasetsand modelused, and describes the describes the datasets, model, and reconstruction method. Section 3 outlines our presents the main results, including the assessment evaluation of Lagrangian water vapor reconstructions and the analysis of LCPs. Section analysis of dehydration regions. Section 4 discusses the potential causes of biases in the Lagrangian reconstruction results and relations examines possible causes of reconstruction biases and their links to convection. Section 5 provides summarizes the conclusions.

2 Data and Method Methods

2.1 Satellite observations

2.1.1 MLS

95

100

105

The Microwave Limb Sounder (MLS) instrument on the Aura satellite Waters et al. (2006) has been providing global measurements

of various atmospheric constituents since August 2004, including (Waters et al., 2006) has provided global profiles of water
vapor, ozone, carbon monoxide, sulfur dioxide, nitric acid, and nitrous oxide profiles using radiances from the nearest limb scan
and other trace gases since August 2004 (https://www.earthdata.nasa.gov/learn/find-data/near-real-time/mls). MLS provides a
offers comparatively high sampling with about 3500 measurement profiles per day. HereIn this study, we use version 5.0 (v5.0)
data, which provides provide water vapor profiles in with 2.1–3.5 km vertical resolution (Lambert et al., 2017), with and
about 3.0 km resolution in the lower stratosphere (Read et al., 2007). We focus on water vapor measurements for the month of
August from 2017 to 2019 in the subtropical regions August 2017–2019 in the tropics (35°S–35°N). The For visualization in
Fig. 1, MLS water vapor profiles are then gridded in gridded into 10°× × 20° (latitude× longitude) horizontal grids. For more

× longitude) bins. Further details on MLS water vapor and the retrieval technique see retrieval methods are given in Livesey et al. (2020).

2.1.2 SAGE III/ISS

We focus on the water vapor measurements in the month of August for 2017–2022 in the subtropies for August 2017–2022 in the tropics (35°S–35°N). We added three more years (2020–2022) of the SAGE Note that the periods considered here for the two satellite datasets are different. For MLS, we use the period 2017–2019, whereas for SAGE III/ISS measurements to increase spatial coverage of SAGE III/ISS water vapor. Comparison of the horizontal distributions of SAGE we extend the period to 2017–2022 to ensure sufficient spatial coverage over the considered region. The shorter MLS period is chosen because the large volume of MLS data provides reliable statistics already for this three-year period but makes the trajectory calculations computationally challenging, particularly when large trajectory ensembles are launched for each measurement point (specific numbers of trajectories are now provided in Section 2.3.1). For SAGE III/ISSwater vapor for the 2017–2019 and , extending the period to 2017–2022 periods results in improves the sampling coverage without introducing no significant differences and does not affect the results of our study. The water vapor profiles provided by SAGE relative to 2017–2019 (cf. horizontal water vapor distributions in Fig. 1 and Fig. S1), thereby justifying the use of the longer period in the analysis.

The SAGE III/ISS v5.3 product are originally water vapor profiles are retrieved on a 1.0 km grid and interpolated on a to 0.5km grid km from 0.5–60.0km in altitude. In this study, we perform km altitude. Following Davis et al. (2021), we apply a 1-2-1 vertical smoothing on all SAGE III/ISS water vapor profiles on a the 0.5km grid following Davis et al. (2021), resulting in km grid, yielding a final vertical resolution of 2km. The profiles are presented in units of number density. We convert the units into mixing ratio using temperature and pressure profiles from the Modern-Era Retrospective analysis for Research and Applications, Version 2 (MERRA-2). Binned data used here for presenting horizontal distributions are gridded with resolution

of-km. For the horizontal distributions shown in Fig. 1, the data are binned at $10^{\circ} \times \times 20^{\circ}$ (latitude \times longitude) x longitude. Tesolution, requiring at least 5 profiles in each bin. We follow the similar procedure described in Park et al. (2021), where SAGE five profiles per bin, following the approach of Park et al. (2021) for SAGE III/ISS v5.1 was used.

155 **2.2 OLR**

We use daily mean outgoing longwave radiation (OLR) as a proxy for deep convection. The OLR data is are obtained from the National Oceanic and Atmospheric Administration (NOAA) Climate Prediction Center (CPC) (https://psl.noaa.gov/data/gridded/data.cpc_blended_olr-2.5deg.html). The CPC blended OLR Version 1 dataset is constructed by blending the level combines Level 2 OLR retrievals from NASA's Cloud and Earth Radiant Energy Systembroadband measurements, NOAA/NESDIS Hyperspectral measurements, and High-resolution Infrared Radiation Sounder measurementsdata. The gridded daily OLR from NOAA covers the period from 1991 to the most recent date, present on a 2.5°× × 2.5° (latitude× × longitude) global grid . We subtract the monthly averages and also provides temporal anomalies, defined as deviations from the monthly mean at each grid pointto obtain the OLR anomalies. The OLR indices used in this study are calculated by averaging the OLR anomalies within specific regions. For . To derive OLR indices for the ASM, the indices are defined as followswe average the temporal anomalies within two horizontal boxes following Randel et al. (2015): (i) an OLR-West :-box covering 20–30°N, 50–80°E, and (ii) an OLR-East :-box, covering 20–30°N, 80–110°E. This separation of convective regions in the ASM follows Randel et al. (2015), and our results are not sensitive to the exact separation longitude. For the OLR values shown in Fig. 8, we use the original values instead of anomalies. Note that, while OLR is a commonly used proxy for convective intensity, it has limitations in identifying deep convection due to its reliance on infrared measurements. These measurements can underestimate cloud-top temperatures, particularly over land and for aged anvil clouds (Liu et al., 2007).

2.3 Models

165

180

2.3.1 CLaMS trajectory module

The Chemical Lagrangian Model of the Stratosphere (CLaMS) is an advanced modeling framework designed for simulating the offline Chemistry Transport Model (CTM) for simulating transport and chemical processes in the atmosphere (McKenna et al., 2002; Konopka et al., 2022). It CLaMS employs a Lagrangian approach, where framework in which individual air parcels are trackedindividually, allowing for a detailed and accurate, enabling detailed representation of atmospheric dynamics and chemistry. For particularly in regions of strong gradients. In this study, we use the trajectory module of CLaMS 2.0, which specifically focuses on the trajectory calculations of air parcels for the calculation of air parcel trajectories (https://clams.icg.kfa-juelich.de/CLaMS/traj). The driving meteorological fields for these simulations are from ERA5, with 1°× × 1° (latitude × longitude) horizontal resolution, 137 vertical hybrid layers, and 6-hour time interval (Hersbach et al., 2020) -temporal resolution (Hersbach et al., 2020). We perform 180-day back-trajectory calculations for air parcels, with backward trajectory calculations, launching each air parcel launched from the precise from the exact spatial location and time corresponding to the satellite data profiles of the satellite observations within the tropics -For each August from 2017 to 2022, SAGE(30°S–30°N).

For August 2017–2022, SAGE III/ISS provides 149, 203, and 2292 profiles for the ASM, NAM, and tropics, respectively. For each August from 2017 to 2019 August 2017–2019, MLS provides 7801, 10,223, and 126,981 profiles for the ASM, NAM, and tropics, respectively. Taking the ASM and SAGE III/ISS observations as an example, the number of calculated trajectories is determined given by 149×10 (profiles \times × altitude levels) for the simulation experiment with one trajectory launched at each measurement point (termed LAG singleexperiment (for the definition of the different model experiments, see Sect. 2.3.2) and 2.3.2 for definitions of the experiments). Likewise, the number of trajectories is $149 \times 10 \times 51$ (profiles \times levels \times ensemble trajectories × altitude levels × trajectory ensemble size) for the LAG experiment experiment with trajectory ensembles started 190 at each measurement (LAG). Accordingly, the total number of ealeulated trajectories for trajectories for the single trajectory experiment LAG single is 1490 for the ASM, 2030 for the NAM, and 22,920 for the tropics, while for LAG, the trajectory ensemble experiment (LAG) these values increase to 75,990, 103,530, and 1,168,920, respectively. Similarly, for MLSthe number of trajectories for LAG single is For MLS, the corresponding numbers of trajectories are 39-,005 for the ASM, 51-,115 for the NAM, and 634,905 for the entire deep tropics, while for the LAG experiment tropics in the LAG single experiment. In 195 the LAG experiment, these values are multiplied by 51, resulting in significantly larger trajectory ensembles, yielding 1,989,255 for the ASM, 2,606,865 for the NAM, and 32,379,155 for the tropics, respectively.

2.3.2 Water vapor reconstruction

We reconstruct water vapor eoneentrations by identifying the cold point temperature. From the local perspective, cold points are the lowest temperatures observed along local vertical profiles. From the Lagrangian perspective, the cold points are defined as the minimum temperatures encountered along the back-trajectories of air parcels, after interpolating the ERA5 temperature and pressure data along the back-trajectoriesmixing ratios from saturation at the coldest temperature and the corresponding air pressure along the trajectories. The reconstructed stratospheric water vapor eoneentrations are calculated using the following formulas: $H_2O_{ppmv} = 1.0 \times 10^6 \cdot e_{sat}/(P - e_{sat})$, where the saturation vapor pressure e_{sat} is given by $e_{sat} = 10^{\left(\frac{A}{CPT} + B\right)}/100$.

Here, mixing ratios are calculated as:

$$H_2 O_{
m ppmv} = 1.0 \times 10^6 \cdot \frac{e_{
m sat}}{P - e_{
m sat}}, \quad e_{
m sat} = \frac{10^{\left(rac{A}{T} + B
ight)}}{100},$$

215

where A = -2663.5, B = 12.537, CPT is the cold point temperature in KT is the coldest temperature (K), and P is the pressure in hPa(Sonntag, 1994). the corresponding pressure (hPa) (Sonntag, 1994).

In the following, we We present results from our experiments based on three types of reconstructions:—, termed LOC, LAG_singleand LAG. (a) LOCuses the minimum temperatures along the vertical profiles associated with SAGE, and LAG, with the following characteristics:

In LOC, T is defined as the minimum temperature in the ERA5 vertical temperature profile at the location of each
 SAGE III/ISS , which are derived from MERRA-2 reanalysis. These minimum values are treated as local cold point
 temperatures (CPTs) and are used in the previously introduced equations to calculate the reconstructions. (b) For water
 vapor profile.

- In LAG_single, back-trajectory simulations are initialized on each measurement backward trajectories are initialized at each observation point in the UTLS, using the its observed altitude, longitude, and latitude that point. Upon obtaining the trajectories, we then find the LCP temperatures to calculate the reconstructions at all the observation points. For the SAGE, T is the LCP temperature, i.e., the minimum temperature along each trajectory, and is then used to compute the water vapor reconstruction at that observation point as described above. For SAGE III/ISSdataset, we set the starting points at altitudes ranging, initialization altitudes range from 14.0 km to 21.0km, with a km at 0.5km interval. For the MLSdataset, we convert pressure to geopotential height then used the one km intervals. For MLS, pressure levels are converted to geopotential heights, and the levels closest to the SAGE III/ISS altitude. (c) For LAG, each measurement point is reconstructed using an even larger ensemble of trajectories by initiating altitudes are used.

220

240

In LAG, reconstructions are based on larger trajectory ensembles. For each observation point, 50 additional starting points vertically spaced at 10-meter launch points are placed vertically at 10 m intervals above and below the observation point. This results in a total of altitude of the observation, resulting in 51 trajectories, including the original one at the observation point. The reconstruction is then based on the ensemble of these back-trajectories in total. For example, if the observation point is at 16.0km (as in the SAGE km (SAGE III/ISSdataset), we set the starting point at 16.0 km and add 50 more points from 15.25 km to 16.25 km, with), the ensemble covers 15.75–16.25 km in 0.01km (10 meters) interval km steps. The final reconstruction values for this for each observation point is calculated obtained by averaging the reconstruction values from H₂Q_{ppmy} values computed from the LCP temperatures along all 51 back-trajectories, to enhance backward trajectories, thereby enhancing the vertical sampling around the original observation point. The final reconstruction value is obtained by averaging all the reconstructed back-trajectories. This dense sampling enhances the vertical resolution of the reconstruction. We specifically increase vertical sampling because observation altitude.

In LAG, the refinement of sampling is applied in the vertical direction, as vertical wind shear generally leads to induces a stronger redistribution of air parcels compared to than horizontal shear. As air parcels move, they are rapidly stretched into thin and horizontally extended layers due to quasi-isentropic quasi-horizontal, isentropic flow. This horizontal spreading gradually dilutes the parcels and lessens the necessity for denser horizontal sampling. Also, given the vertical resolution of MLS and SAGE III/ISS data (3 km and 2 km, respectively), it is more important to increase the vertical sampling in our trajectory calculations to better reconstruct the water vapor mixing ratios. For further details of these processes, please refer to Haynes and Anglade (1997), which explains how differential advection in the atmosphere drives vertical mixing and stretching of air parcels.

All the back-trajectories are categorized backward trajectories are classified into two groups: those that cross the tropopause are ascend through the tropopause into the stratosphere, referred to as Troposphere-to-Stratosphere Transport (TST), and those that do notare, referred to as non-TST. TST trajectories are defined as those with starting points (or trajectories with launch points (observation points) located above 370 K potential temperature and that can be traced back to below 340 K potential temperature. For TST trajectories, the reconstructed water vapor concentrations mixing ratios are calculated using the LCP temperatures. For non-TST trajectories, the reconstructed values are defined as the smaller of the two two quantities: the

saturation mixing ratios ratio based on LCP temperatures, and the climatological water vapor concentrations mixing ratio from MLS at the carliest back-trajectory endpoints simulated origins of the backward trajectories, following the procedure of Fueglistaler et al. (2005).

3 Results

260

265

280

3.1 Performance of Lagrangian water vapor reconstruction

255 3.1.1 Spatial distributions

Both the ASM and NAM regions show enhanced water vapor mixing ratios based on satellite observations during boreal summer. Figures Figures 1a and 1b show present the horizontal distributions of water vapor satellite observations in August at ~16.5 km (around 100hPa pressure level—hPa or 380K potential temperature level)based on SAGE K), observed by SAGE III/ISS and MLSsatellite observations, respectively. The distributions from both satellite datasets show consistent spatial patterns, with the moisture maxima located over the ASM (15°–35°N, 50°–150°E) and NAM (10°–35°N, 160°–80°W). The high values from SAGE III/ISS (exceeding 7 ppmv) are higher than the values from MLS (5–6 ppmv). Figure 1c and 1d present reconstructed water vapor derived from ensemble trajectories (Experiment LAG), where more than 80% of the trajectories are classified as TST (Sect. 2.3.2), based on the profiles from SAGE III/ISS and MLS, respectively, corresponding water vapor reconstructions (experiment LAG). Overall, the reconstructions exhibit a noticeable dry bias across the entire tropics compared to the observations. Concerning the spatial patterns, however, the water vapor distributions reconstructed from trajectories for the two. The reconstructions show dry biases across the tropics relative to observations. Except for the maxima over the NAM, the spatial patterns from both satellite datasets are similar, in particular showing elevated mixing ratios above the ASM, similar as in the satellite observations. While the elevated water vapor mixing ratios in the ASMare captured, the observed moist anomaly in the NAMis not reconstructed from trajectories broadly reproduced, particularly over the ASM.

The anomaly fields (Fig. 1e-h) highlight these features more clearly. Over the ASM, the reconstructions capture the magnitude of the observed enhancement (1–2 ppmv) but with a more limited spatial extent, whereas over the NAM, the reconstructions only weakly reproduce the observed moisture enhancement by less than 1 ppmv. The observed anomalies from SAGECompared with MLS, SAGE III/ISS are ~1–2 ppmv over the ASM and NAM observations show higher water vapor mixing ratios by ~1 ppmv across most tropical regions (Fig. 1e), which is higher than the those from the MLS (1a, b), as well as larger moisture enhancements of ~1ppmv) as shown in Fig ppmv above the ASM and NAM in the anomaly feilds (Fig. 1e, f). 1f. Compared to the observations, the reconstruction successfully captures the water vapor anomalies over the ASM (1–2 ppmv), covering smaller area. However, the reconstruction over the NAM shows an increase of less than 0.5 ppmv in water vapor concentrations, with the maximum located near the equator.

Figure 2 analyzes 2 shows the vertical structure of the observed and reconstructed water vapor profiles, averaged over the three regions of interest: tropics, ASM, and NAM. All water vapor profiles show a decrease in concentration from the troposphere to the UTLS region. The variability in water vapor is greater in the troposphere Consistent with the observations,

the water vapor reconstructions in the UTLS exhibit higher mixing ratios and variability than in the stratosphere. The reconstructed profiles partially capture these distinct characteristics of water vapor in both the troposphere and stratosphere, in terms of both concentration and variability.

285

290

295

300

305

310

315

In the tropics (Fig. 2a-b), the cold point tropopause and the lapse rate tropopause are located at 16.7 km (evan dashed lines) and 15.7 km (vellow dashed lines), respectively. Below the lapse rate tropopause, the reconstructed profiles 2a-b), the reconstructions (blue lines) based on SAGE both SAGE III/ISS show maximum dry biases of -2.3 ± 2.5 ppmy at 15.5 km, while MLS-based reconstructions exhibit biases of -1.5 ± 1.5 ppmy at and MLS have ~15.1 km. Within the tropical tropopause layer (between the cold point and lapse rate tropopauses) 1–2 ppmy dry biases in the upper troposphere, likely due to missing cloud microphysics and convective moistening in the reconstruction (cf. Schiller et al., 2009). With increasing altitude, both the magnitude and variability of the dry biases gradually decreasewith increasing altitude. Above biases decrease, stabilizing above the cold point tropopause, the dry biases decrease to . At 17.0 km (SAGE III/ISS), the biases are -1.7 \pm 0.7 ppmv $(-34\% \pm 14\%)$ at 17.0 km based on SAGE III/ISS, and to , and at ~17.4 km (MLS), they are -0.8 \pm 0.6 ppmy (-21% \pm 15%)at ~17.4 km based on MLS. Similar dry biases have been reported by Liu et al. (2010), who found that stratospheric water vapor predictions. Comparable magnitudes of dry bias have also been reported in reconstructions based on the saturation mixing ratio at the Lagrangian dry point of trajectories exhibit dry biases of up to -50% ± 10%, which they advection condensation paradigm (Liu et al., 2010), attributed to missing cloud microphysics, Above 19.0 km, the biases in the reconstructions are 1-2 ppmv smaller when both TST and non-TST trajectories are considered (Fig. S2), compared to when only TST trajectories are used (Fig. 2). The black diamonds in Fig. S2 represent the percentage of TST trajectories relative to the total number of trajectories, indicating that non-TST trajectories account for more than 95% above 19.0 km. This suggests that water vapor concentrations in the higher stratosphere align more closely with climatological values and less with direct transport from the upper troposphere within 180 days.

In monsoon regions, the main structures of both observed and reconstructed profiles are similar to those in the tropics, though there are some noticeable differences. From the observed profiles, UTLS water vapor concentrations in monsoon regions are higher than in the entire tropics, especially below the lapse rate tropopause. The anomalies of observations, compared to the average in the tropics, reach 4.5 ppmv at 16.5 km for the ASM (Fig. 2e) and 1.5 ppmv for the NAM (Fig. 2e), as derived from SAGE III/ISS observations.

In the ASMregion, the tropopause layer is higher and thinner (16.6–17.1 km) compared to that in the tropics. For the reconstructions based on SAGE III/ISS, the reconstructed ASM profiles have substantial dry biases below the lapse rate tropopause, up to -4.9 ± 4.2 ppmv at 15.5 km, significant moistening is observed, particularly in the upper troposphere. The reconstructions reproduce part of this moistening but retain pronounced dry biases (Fig. 2e–d). However, these biases gradually decrease with altitude, reducing to -1.7 ± 0.8 ppmv at 17.5 km, consistent with the bias levels seen in the tropics 2b, e). To further assess the vertical performance of the reconstruction, we compare the reconstructed ASM anomalies. The contrast between the coral and grey bars in the right sub-panels illustrates how well the moisture enhancements relative to the entire tropic tropical mean are captured. At 15.5 km, the SAGE-based reconstructions capture approximately reconstructions based on SAGE III/ISS reproduce about one-third of the observed anomalies (Fig. 2b; right sub-panels). The agreement improves

significantly with altitude: enhancement magnitude. Agreement improves with altitude, exceeding two-thirds at 16.5 km, the reconstructed anomalies account for over two-thirds of the observed values, and above this level, the reconstructions approach even closer agreement. Similar results are also reflected in the MLS-based reconstructions and approaching close consistency above this altitude. Similar behavior is found in reconstructions based on MLS (Fig. 2e; right sub-panels). This shows that the Lagrangian reconstruction method performs reliably above tropopause levels. The consistent behaviour of the reconstruction in the ASM compared to the tropics further suggests.). The resemblance between ASM and tropical reconstructions indicates that stratospheric water vapor mixing ratios above the ASM is primarily governed by the mechanisms freeze-drying in the large-scale temperature field ('advection-condensation' paradigm, see Liu et al., 2010)—are well explained by the advection-condensation paradigm, as in the deep tropics. In contrast, at lower altitudes in the tropospheretropospheric altitudes, water vapor is likely more strongly influenced by other processes such as deep convection. Consistent with our findings, Plaza et al. (2021) showed that while convection can moisten the upper troposphere ; its signature could be erased but that this signal may be removed by subsequent dehydration at higher altitudes. As a result, convection plays a limited role in determining water vapor concentrations in the lower stratosphere of monsoon regions, whereas small-scale mixing appears to be a more dominant contributor. levels.

In the NAM, the tropopause layer (15.6–16.5 km) is slightly lower and thinner compared to that in the tropics (Fig. 2e

In the NAM, the tropopause layer (15.6–16.5 km) is slightly lower and thinner compared to that in the tropics (Fig. 2e and 2f). As the altitude increases, the bias profile The profiles for the NAM tell a different story. At 17.0 km, within the stratosphere, the reconstruction bias remains -1.8 ± 1.2 ppmv based on SAGE III/ISS decreases more slowly than in the ASM, with a remaining bias of -1.8 ± 1.2 ppmv at 17.0 km within the stratosphere (Fig. 2c). Moreover, the fraction In addition, the fractions of the observed anomaly enhancements captured by the reconstruction is considerably reconstructions are much lower in the NAM compared to both the ASM and than in either the ASM or the tropics (Fig. 2eand 2 2c, f; right sub-panels). The distinct structure of the tropopause layer and the corresponding reconstruction performance performance of the reconstructions in the NAM suggest that considering only the freeze drying effect by advectionthrough the large-scale temperature field (as represented in the Lagrangian reconstruction method) is insufficient to explain the moist anomaly in the NAM region. Hence, further processes like suggests that the advection—condensation paradigm alone can hardly explain the observed moisture enhancement. Additional processes such as convection, mixing, and ice microphysics are likely to likely play a more significant role in important role in controlling stratospheric water vapor variability in the NAMthis region.

Comparing the profiles from SAGE III/ISS (left) with those from MLS (right), the higher vertical resolution profiles from SAGE III/ISS show more strongly enhanced water vapor concentrations and clearer peak values in the UTLS for the three regions of focus, especially the ASM. The reconstructions based on SAGE III/ISS and MLS resemble each other. The SAGE III/ISS dataset, with its higher vertical resolution, captures more features of water vapor variations in the UTLS, while MLS may lose information due to lower vertical resolution. However, the limited and uneven sampling of SAGE III/ISS might restrict its ability to reveal spatial features, which could be the main reason for the slight differences between the reconstructions based on the two datasets.

3.1.2 Lagrangian reconstruction sensitivities

To assess the performance of the reconstructions from different experiments, we present the To evaluate reconstruction performance across experiments, Fig. 3 shows correlation coefficients between observed and reconstructed water vapor concentrations in Fig. 3. mixing ratios. In addition to the Lagrangian reconstruction using cold point temperatures from ensemble trajectories large trajectory ensembles (LAG) based on both SAGE III/ISS and MLSdatasets, we also include the reconstruction using cold point temperatures from individual trajectories (, results from LAG_single) and the reconstruction using local cold point temperatures (LOC) only and LOC based on SAGE III/ISS profiles. This allows a direct comparison of the Lagrangian methods with the local perspective. Note that the are also included. The x-axis in each plot shows the length of indicates the backward period used for length used in the trajectory calculations, thus the correlation coefficients for LOC; hence, the LOC values remain constant.

The reconstructions from LAG exhibit the highest correlation show the highest correlations with observations, followed by LAG_single, while LOC shows the lowest correlation coefficients: -0.12 in the tropics, 0.07 in the ASM, and -0.17 in the NAM.-values. As expected, using local cold point temperatures to determine stratospheric water vapor yields unreliable results (compare Fueglistaler et al., 2005). Similarly, produces unreliable results (cf. Fueglistaler et al., 2005). Reconstructions using smaller trajectory ensembles (LAG_single) have limited accuracy, as trajectory reconstructions are highly are less accurate than using large ensembles (LAG), as the reconstruction is sensitive to the initial air parcel position and to small variations in wind and diabatic heating fields. By averaging over larger trajectory ensembles (LAG), the reconstruction becomes more robust and accurate, effectively capturing the inherent uncertainties in the systemrates. For the results reconstructions based on MLS and SAGE III/ISS, changing the the choice of dataset does not significantly affect reconstruction performance across the three regions. This suggests that the results based on SAGE III/ISS are generally representative and reliable for the purposes of this study, despite its lower horizontal and temporal sampling compared to MLS.

365

370

375

The Lagrangian reconstruction of water vapor using the Lagrangian method aims to find identifies the minimum saturation mixing ratio along the trajectory, and therefore the backward time length of the simulation might influence the results—trajectories, making the simulation results sensitive to the backward simulation length. As shown in Fig.—3, all Lagrangian experiments display a consistent increasing trend in correlation coefficients as the backward calculation time increases. For instance increasing correlation coefficients with longer backward periods. For example, in LAG (SAGE III/ISS), the correlation coefficients for the ASM region increase increases from 0.53 (with a 60-daybackward period) to 0.69 (with a 180-daybackward period), and for the NAM from 0.43 to 0.75 for the NAM. The most rapid increase occurs when extending the backward period from—with the steepest rise occurring between 60 to and 120 days. These significant improvements in the reconstruction suggest. The improvements in correlation indicate that UTLS water vapor concentrations mixing ratios in August are partially partly influenced by processes from boreal spring or even winter, particularly at higher altitudes—where the time periods elapsed since air parcels had encountered their LCPsmay be months. Such where it needs months for air parcels to sample their LCPs. This delayed influence is also well-known in the context of the atmospheric 'tape recorder', where water vapor consistent with the atmospheric "tape recorder" in which anomalies imprinted at the cold point propagate upward due to the with weak tropical upwelling (Mote et al., 1996). Within the ASM anticyclone, weak mixing allows this memory effect to be preserved

along upward-moving trajectories, which is also referred to as 'upward spiraling' (Vogel et al., 2019). preserves this memory along ascending trajectories, a process often described as "upward spiraling ascent" (Vogel et al., 2019).

In general, it is known that the Lagrangian temperature history is necessary to explain the dehydration process in essential for explaining dehydration near the tropical tropopause layer and the observed and the resulting dryness of the lower stratosphere (Fueglistaler et al., 2005). However, in the Northern hemisphere monsoon circulations however, air masses are confined to some degree and it is not clear per se if partly confined, and it remains unclear whether dehydration and moistening processes are controlled more strongly are governed primarily by local processes (e.g., convectionin the monsoons). To investigate thisquestionsuch as monsoon convection. To address this, Fig. 4 shows correlations of the SAGE 4 compares correlations of SAGE III/ISS and MLS water vapor values observed in UTLS against in the UTLS with local cold point temperatures and against LCP temperatures, respectively. Clearly, the correlation between with LCP temperatures.

The correlation between the observed water vapor concentrations and mixing ratios and the local cold point temperatures is very weak (Fig. 4a - e 4a - e), and the saturation values calculated using local cold point temperatures saturation values derived from them (grey points) show large moist biases compared to observed values: 15.14 ppmv on average relative to observations: 13.89 ppmv in the tropics, 6.16-5.85 ppmv in the ASM, and 13.48-13.80 ppmv in the NAM. In contrast, the correlations between water vapor concentrations and LCP temperatures are much stronger, ranging from 0.60 for the ASM based on the SAGE III/ISS dataset correlations with LCP temperatures, as derived from the trajectories, are much stronger (Fig. 4e) to 0.78 for the NAM region (Fig. 4f). The 4e, f) and the reconstructed water vapor biases are also significantly reduces to ~1–2 ppmv (but dryer) on average for dryer by ~1–2 ppmv across all regions.

Hence, we find a similarity between the monsoon regions and the deep tropicsregarding the correlation between observed lower stratospheric water vapor mixing ratios and LCP temperatures, but not These results show that, as in the tropics, UTLS water vapor in the monsoon regions correlates strongly with LCP temperatures rather than with local cold point temperatures derived from reanalysis. This suggests indicating that dehydration in these regions is likely primarily governed by non-local processes associated with large-scale transport. However, we note that overshooting convection—often considered a direct injection mechanism pathway for water vapor into the lower stratosphere—is a sub-grid scale process not fully resolved in reanalysis. Therefore, using local cold point temperatures may underestimate the advection-condensation approach based on large-scale temperature and wind fields likely underestimates the impact of such events convection, and the weak correlation with local temperatures might does not entirely rule out the role of a role for local processes in the monsoon regions.

The regression lines for observations versus LCP temperatures (blue lines) in Fig. 4d–i all have smaller slopes than those for the saturation mixing ratios (grey lines), likely due to the influence of points above 19.0 km. Above this altitude, air is more likely to be well-mixed within the stratosphere, making water vapor concentrations less correlated with LCP temperature and more representative of climatological moisture conditions (Fig. S2). The ASM and NAM regression slopes from SAGE III/ISS (Fig. 4e–f) are closer to the saturation slopes, likely due to less sampling at high altitudes. Moreover, tracing air parcels back to the troposphere becomes more uncertain at higher altitudes, as longer back-trajectories introduce greater uncertainties in LCP determination.

3.2 Locations of the Lagrangian cold points Dehydration regions

430

435

440

445

The Lagrangian reconstruction not only reproduces observed water vapor values but also traces the regions where dehydration occurred before reaching the observation points. Since dehydration events can take place weeks to months earlier, it is crucial to identify the dominant locations of these events and assess whether they are concentrated in specific regions or more broadly distributed across the tropics. Utilizing all back-trajectories (from experiment LAG), we trace the observations back to the specific locations of their LCPs. Given the large number of such trajectories, we calculate the spatial distribution of these locations using Figure 5 shows the spatial distribution of LCPs, and Fig. 6 presents the corresponding probability density functions (PDFs). The scatter plots of the locations of LCPs are shown that highlight the main dehydration regions. The left panels in Fig.5 (with colors denoting the reconstructed water vapor values), and the corresponding PDFs are presented in Fig. 6.

The results from the SAGE 5 show results based on SAGE III/ISSand MLS datasets show similar patterns for both monsoon regions. In the ASM region (Fig. 5c-d), LCPs are spread across the 0–30°N zonal band, with most dehydration points situated in the ASM region and some extending into North Africa and North America. According to the PDF of the LCPs in. Overall, the LCPs are largely confined within the tropics. For the ASM (Fig. 6e-d, most of the LCPs are located over India and the Bay of Bengal, around 10°–30°N, 70°–95°E, indicating the primary origin of reconstructed water vapor in the ASM. For the top 10% of the highest reconstructed water vapor concentrations (exceeding –6 ppmv), the LCPs are concentrated in the same region (red contour lines), slightly displaced towards higher latitudes. This suggests that the increased water vapor in the ASM, as determined by the reconstruction method, is primarily attributed to dehydration processes occurring in the vicinity of the monsoon over South Asia. According to Konopka et al. (2023), 5c), the 'dehydration carousel' mechanism within the ASM anticyclone plays a key role in shaping the distribution of water vapor entering the stratosphere, that is, while deep convection supplies moisture to the upper troposphere, the coldest regions near the monsoon's southern vicinity act as primary dehydration sites LCPs cluster near the monsoon region, and show high reconstructed mixing ratios consistent with the elevated cold point temperatures. In the case of the NAM (Fig. 5e), although some LCPs are situated in its vicinity, a considerable portion is concentrated over southern Asia. The results based on MLS show similar features (Fig. 5b, d, f).

The PDFs (Fig. 6) highlight the main dehydration regions. Regardless of whether air parcels end up in the ASM, NAM, or across the tropics, southern Asia emerges as the dominant dehydration region for tropical UTLS air, consistent with previous studies (Fueglistaler et al., 2004; Ploeger et al., 2013; Schoeberl and Dessler, 2011). Air parcels that undergo dehydration in these regions can later be transported dehydrated in the ASM can then circulate within the anticycloneand, ascend into the stratosphere, contributing to the observed high water vapor concentrations in the lower stratosphere.

The backward time length required for air parcels observed at 16.5km to reach these LCPs is shown in Fig. S3a-b, indicating that the dehydration processes occur over a timescale of days to weeks before the air parcels reach the observation points. Other LCPs, located further away and with lower reconstructed water vapor concentrations (1–5 ppmv), correspond to longer time periods (1–6 months) between the dehydration event and observation. While these air parcels with low water vapor are not the primary factor for the monsoon moist anomalies, their contribution to the water vapor budget highlights the need to extend the

simulated backward time period, especially considering the improvements in correlation coefficients shown in Fig. 3. These findings reinforce the idea that the ASM anticyclone serves as a crucial transport pathway for air into the stratosphere, while dehydration near its vicinity regulates the amount of water vapor that ultimately enters the stratospheric circulation.

For the NAM region and contribute to enhanced lower stratospheric water vapor (Konopka et al., 2023). The red contours further show the PDFs for the top 10% of reconstructed water vapor mixing ratios. For the ASM (Fig. 5e-f), a significant number of LCPs are observed across North America. Remarkably, the region of occurrence of LCPs extends throughout the 0-30°N zonal band even into southern Asia. The PDFs in Fig. 6e-f indicate that the primary dehydration center is in the ASM region, meaning that most air parcels in the NAM experienced dehydration in southern Asia. Focusing on the top 10% highest reconstructed water vapor concentrations 6c-d), the moistest air is primarily dehydrated locally. For the NAM (Fig. 6e-f), we identify two leading centers for the LCPs. One center is located two dominant dehydration centers emerge: one in southern Asia , a similar region to the ASM dehydration center but displaced slightly southeastward. The other, more significant center is and another, more pronounced, near the NAM itself, which is likely the main contributor to the increase in reconstructed water vapor concentrations in the NAM. This suggests that the increase in reconstructed water vapor concentrations. These results suggest that stratospheric air in the NAM region is primarily influenced by local tropopause temperatures, with additional moisture contributions from transport from southern Asia, is largely dehydrated remotely over southern Asia, while the moistest mixing ratios are shaped by both remote transport and local processes. In the trajectory simulations, the average backward period required to trace observed air parcels back to their LCPs for the NAM is ~45 days (Fig. S3c-d). This indicates that the temperatures used to reconstruct the water vapor at those LCPs are partially from June or even earlier, which are lower than the temperatures in August, leading to lower reconstructions.

The locations of LCPs for the tropics (Fig. 5a–b) resemble an ensemble of those found in the ASM and NAM, suggesting that dehydration predominantly occurs near the monsoon regions. Additionally, the PDFs for the tropics (Fig. 6a–b) show that LCPs are highly concentrated in southern Asia, even when considering only the top 10%, reinforcing the significance of southern Asia as a major dehydration center of the monsoon regions.

3.3 Lagrangian reconstruction and convection

455

460

465

475

480

485

We further investigate examine the relation between the dry bias in the reconstructions and convection as a potential moistening process. Therefore, we follow Following recent studies (e.g., Randel et al., 2015; Peña-Ortiz et al., 2024)and, we use OLR as a proxy for convectionintensity, with high OLR values corresponding to weak convection and low OLR values corresponding to strong convection. Note that while OLR is a commonly used proxy, it has limitations—it primarily, with low (high) OLR values indicating strong (weak) convection. It should be noted that, while widely applied, OLR mainly captures cold cloud tops and may miss warm-topped or thin convection, leading to potential biases in certain regions or conditions (e.g., Liu et al., 2007).

Randel et al. (2015) used thin convection with warm cloud tops, which can introduce regional biases (e.g., Liu et al., 2007).

Randel et al. (2015) analyzed MLS observations from May to September (2005–2013) to obtain time series of UTLS (2005–2013) to derive water vapor time series in the ASM UTLS (specifically at 100 hPa) water vapor concentrations in the ASM, separating specific, and further separated wet and dry phases to reveal the corresponding anomalous convection patterns. Their findings

indicate that convection exhibits a west-east dipole structure over the whole ASMregion. The strong convection over associated convection anomalies. They identified a west-east dipole structure in convection across the ASM, likely linked to different modes of the ASM anticyclone (Honomichl and Pan, 2020). Strong convection in the eastern part of the dipole (20–30monsoon region (20–30°N, 80–11080–110°E) corresponds to a dry phase in the ASM UTLS (i.e. low UTLS water vapormixing ratios over the whole ASM)corresponded to dry UTLS phases (low ASM water vapor), and vice versa. We conduct a similar analysis to derive OLR indices and then composite water vapor concentrations within the entire ASM region (15–35°N, 60–140°E) for observations from SAGE III/ISS and the reconstructions. Two OLR indices are defined according to the dipole structureBuilding on the method used in Randel et al. (2015), we derive two OLR indices to represent convection intensity in the ASM: an OLR-West index quantifies convection intensity in for the western part , while and an OLR-East index quantifies convection intensity in for the eastern part of the ASM (Sect. 2.2). These indices are used to select days with relatively weak convection (OLR ≥ 1.5 standard deviations) and strong convection (OLR Using these, we composite reconstructed and observed (SAGE III/ISS) UTLS water vapor mixing ratios for the ASM region (here defined as 15–35°N, 60–140°E). Days of strong and weak convection are identified as OLR temporal anomalies ≤ -1.5 standard deviations). The west-east shifts in convection, as reflected in these OLR indices, may be related to different modes of the ASM anticyclone (Honomichl and Pan, 2020)and ≥ +1.5 standard deviations from the mean, respectively.

Figure 7 presents 7 shows water vapor observations and reconstructions averaged over the 0–10 days following strong and weak convection eventsdays. The composites for convection intensity in For the eastern part of the ASM reveal, composites indicate that observed water vapor mixing ratios are drier for lower on strong-convection days than those composited for on weak-convection days below 17.5 km (Fig. 7a). This drying effect of convection is weak within the The drying effect is weak in the lower stratosphere at 17.5 km (-0.21 ppmv) but increases to -6.6 ppmv more pronounced at 15.5km within troposphere km in the troposphere (-6.6 ppmv). Conversely, the composites for convection intensity in In contrast, composites for the western part of the ASM show the opposite trend: composited water vapor concentrations for pattern: water vapor mixing ratios are higher on strong-convection periods are higher than those for days than on weak-convection periods days below 17.5 km (Fig. 7b). Our These results are consistent with Randel et al. (2015), demonstrating indicating that strong convection in the eastern part of the ASM is associated with ASM is linked to a dry UTLS, whereas a westward shift of strong convection is associated with a moist UTLS.

The right panels of Fig. 7 display 7 show the reconstructed water vapor profiles. Below the lapse rate lapse-rate tropopause (yellow dashed lines), the reconstructions show an insignificant display little response to changes in convection intensity compared to the observations. This finding suggests, indicating that the reconstruction is not capable of catching method cannot capture the influence of the west-east shift of convection west-east convection shift in the ASM region. These differences between the reconstruction and observations concerning the effect of convection in the ASM region highlight a The discrepancy underscores the key limitation of the simple Lagrangian water vapor reconstructionmethod: while it effectively represents large-scale dehydration and transport processes, it struggles to accurately represent reconstruction, that it is not capable of capturing the convective moistening and drying, along with localized processes in the upper troposphere. This limitation is also

evident in Fig. 2b, where the reconstructions exhibit increasing dry biases from less than 2 ppmv in the stratosphere (above 17.5 km) to a maximum of 5 ppmv in the troposphere (15.5 km).

Finally, we investigate potential relations between biases in the reconstruction and the intensity of convection. Figure 8further examines the relation between convection intensity (based on the OLR-indices defined abovea and b show the correlation between reconstruction biases near the lapse rate tropopause (16.5 km) and the biases in reconstructed water vapor concentrations 525 at 16.5 km based on SAGE III/ISS. Overall, convection convection intensity in the eastern part of the ASMis stronger and western ASM, respectively. Convection is stronger in the eastern ASM (OLR 200-230W/Wm²) than in the western part of the ASM (OLR 240–280 W/W m²). However, but it shows no significant correlation of with the reconstruction bias to convection in the eastern monsoon region is found (Fig. 8a), suggesting that eastern convection does not significantly impact the reconstruction performance. In contrast, convection in the western monsoon region exhibits a significant correlation-ASM 530 is strongly correlated with the reconstruction bias, with a correlation coefficient of 0.73 (r = 0.73*, statistically significant at the 95% confidence level; Fig. 8b). Despite being weaker than eastern convection, western convection has a stronger influence on the biases, leading to increased dry biases in the reconstructions following periods of strong convection. This pattern is also evident when comparing Fig. 7b and 7d., indicating that dry biases increase following strong-convection periods in the 535 western ASM. In addition, Therefore, the moistening effect of convection in the western part of the monsoon region (e.g. related to ice injection), which is not included in the simple trajectory reconstruction approach, likely contributes strongly to the reconstruction dry bias. The correlation between the dry biases and the correlation between reconstructed biases and convection intensity in the western monsoon region (OLR-West index) varies-ASM decreases with altitude, with correlation eoefficients of 0.47, coefficients of 0.73*(with a star indicating statistical significance at the 95% confidence level based on 540 the Student's t-test), 0.46, and 0.24 from 16.0 km to 17.5 km (with 0.5 km interval). With the exception of at 16.5 km, the correlations at other levels do not pass the significance test. The correlation maximum 17.0, and 17.5 km, respectively. Except at 16.5 km, correlations are not statistically significant at the 95% confidence level. The strong correlation at 16.5 km highlights the relevance of convection-driven processes km suggests that convection particularly affects the water vapor mixing ratios near the tropopause. We attribute this altitude-dependent behavior to different atmospheric regimes: at and below 16.5 km, 545 convection has a stronger influence, whereas above 17.0 km, the Lagrangian reconstruction becomes water vapor mixing ratios become less sensitive to convection and is dominated are more strongly governed by large-scale transport and the trajectory history of air parcelsprocesses.

4 Discussion

550

As shown in Fig.- 1 and Fig.- 2, the reconstructions exhibit reconstruction exhibits a consistent dry bias (~of about 1.5ppmv) ppmv above the cold point tropopause in both the ASM region and throughout the broader the tropics. A similar dry bias has been bias was reported by Liu et al. (2010), who suggested that incorporating including cloud microphysical processes could significantly reduce this biasby relaxing the assumption of instantaneous dehydration to the saturation mixing ratio. Similarly, Schoeberl et al. (2013) alleviate this bias. Schoeberl and Dessler (2011) implemented a Lagrangian cloud model that

simulates the conversion of excess water vapor to ice, and setting parcels to saturation within convection zones. They showed that including such simplified Lagrangian cloud model improves model that allows a certain degree of supersaturation, and achieved close agreement with MLS observations. Also other studies have shown that a simple allowance Other studies have also demonstrated that allowing for supersaturation at LCPs can substantially reduce the dry bias (Schiller et al., 2009; Ploeger et al., 2011). However, while effective, this approach remains a simplified representation While effective, such methods remain simplified treatments of the complex microphysical processes that influence govern dehydration efficiency, as well as of other small-scale processes like influences such as turbulence and mixing (Poshyvailo et al., 2018). Such underrepresented processes can These underrepresented processes likely contribute to the dry bias in our reconstructions.

While the simplified Lagrangian method performs well in reconstructing the moist anomaly moisture enhancement in the ASM, it struggles with representing to represent the moisture budget in the NAM, suggesting that different mechanisms may be are at play in this region. Previous studies indicate that , in during boreal summer, the ASM is characterized by a strong anticyclonic circulation at 100hPa, along with hPa, accompanied by a smaller, approximately roughly symmetric anticyclone in the Southern Hemisphere subtropics, which can be explained by. These monsoon circulation patterns are consistent with the dynamical structure of the Gill response (Park et al., 2007). In contrast, the geopotential height geopotential height fields over North America at 100hPa exhibits hPa show no such structure, highlighting underscoring a fundamental difference between the NAM and ASM from a large-scale circulation perspective. AlsoFurthermore, studies by Smith et al. (2017) and O'Neill et al. (2021) show that frequent deep convection demonstrate that particularly intense deep convection events over North America and particularly intense convective events, can transport water vapor and ice directly into the lower stratosphere. These findings results suggest that deep, potentially overshooting convection might play a more crucial possibly overshooting convection plays a more critical role in the UTLS water vapor budget in the NAM compared to other regionsthan in other regions, and may be the primary driver cause of the large biases observed in Lagrangian reconstructions.

Additionally, as suggested by our trajectory simulation results, Additionally, our trajectory simulations suggest that long-range transport from southern Asia to the NAM region appears to significantly influence NAM water vapor concentrations. On the one hand, the significant fraction of air masses experiencing dehydration over southern Asia before reaching North America implicates the dominant role of the Asian monsoon in controlling the moisture entering the stratosphere during boreal summer, which is consistent with previous studies (Fueglistaler et al., 2004; Ploeger et al., 2013). On the other hand, significantly influences water vapor mixing ratios in the limited performance of the reconstruction for the NAM may be attributed to errors NAM region, making the reconstructed values sensitive to uncertainties in ERA5 winds, which can introduce biases in transport modeling, temperatures, winds and diabatic heating rates. Additionally, the presence The coexistence of multiple, competing mechanisms within convection events may further complicate the accurate representation of (Homeyer et al., 2024) further adds substantial complexity to representing long-range transport in models (Homeyer et al., 2024). These uncertainties make it difficult to accurately reproduce water vapor mixing ratios over the NAM.

Moreover, previous studies have shown that trajectories computed with 6-hourly reanalysis data exhibit transport errors and warm biases of around the cold point tropopause compared to those trajectories calculated with higher temporal resolution (1-hourly) data (Pisso et al., 2010; Bourguet and Linz, 2022). These biases could lead to inaccuracies in simulating

Such biases can affect the simulation of dehydration processes and ultimately impact, in turn, the reconstructed water vapor distribution. Investigating Incorporating additional tracers originating from Asia could help assess to evaluate whether long-range transport from Asia to the NAM region and its remote influence on NAM water vapor levels are accurately captured are accurately represented in current trajectory-based reconstructions.

5 Conclusions

590

595

600

605

615

620

This study investigates the performance of Lagrangian reconstructions of UTLS water vapor in the boreal summer monsoons monsoon regions over Asia and North America. The reconstructed water vapor fields are evaluated using SAGEdurgin boreal summer based on SAGE III/ISS and MLSobservations, with SAGE III/ISS providing higher vertical resolution and revealing finer-scale structures in the UTLS. Our results demonstrate the effectiveness of the Lagrangian method in capturing tropical UTLS water vapor variations and structures, with improved performance from the tropopause upwards.

Overall, the Lagrangian approach, including the temperature history of air masses, is found to be equally effective in reconstructing water vapor mixing ratios in the Asian monsoon as in the deep tropics. Given that most air parcels undergo dehydration in the southern vicinity of the ASM, we conclude that UTLS water vapor concentrations in the ASM are largely governed by large-scale transport through the cold tropopause in this region. A systematic dry bias in reconstructions in the ASM of approximately, and particularly assesses the performance of related Lagrangian reconstruction approaches. The results show that the Lagrangian reconstructions consistently exhibit a dry bias of about 1.5ppmv is similar to dry biases found previously for lower stratospheric water vapor in the deep tropics. Nevertheless, the Lagrangian reconstruction reproduces the anomalies of stratospheric water vapor mixing ratios—ppmv across the tropics. Despite this, the method reproduces UTLS water vapor variations and structures well in the ASMwell and captures more than two-thirds of the observed moist anomalies. Reconstructions using, but performs poorly in the NAM. Reconstruction skill improves with altitude above the tropopause. Also, larger trajectory ensembles for each satellite observation point show significantly better performance compared to reconstructions based on give more robust results than smaller ensembles.

Conversely, the Lagrangian method fails to reproduce the observed moistening in the NAM region. The ERA5-driven trajectory simulations suggest that while the highest In the ASM, UTLS water vapor concentrations in the NAM mixing ratios are primarily controlled by local tropopause temperatures over America, most air masses in the NAM region are remotely southern Asia. In the NAM, water vapor is strongly influenced by long-range transport from southern Asia and the associated tropopause temperatures there, hence by tropopause temperatures in that region. However, the moistest air masses appear to be locally controlled by temperatures in the NAM region.

We hypothesize that the failure of the water vapor reconstruction in the NAM UTLS is likely due to arises primarily from an underestimation of local moistening processes such as deep convection and ice injection, which are not explicitly included in the reconstruction method. Additionally, errors in the framework. Errors in representing cross-Pacific long-range transport could be another factor affecting likely contribute further to the particularly large dry bias in the NAM reconstructions.

Finally, based on analyses of convective variability, using Using outgoing longwave radiation as an indicator of a proxy for convection, we also assessed the impact of convection on UTLS water vapor variability and on the bias biases in the Lagrangian reconstructions. Based on observations from SAGE Observations from SAGE III/ISS we can confirm the findings of Randel et al. (2015)which show—showing that strong convection in the eastern part of the ASM leads to UTLS drying, whereas a westward shift of convection results in UTLS moistening. These signals, however, are not captured by the reconstructions. Correlation analyses reveal that the biases in Lagrangian reconstructions are significantly linked to the intensity of convection in the western region of the ASM, with stronger convection associated with increased dry biases. In contrast, no clear influence on the reconstruction bias is found for convection in the eastern Correlation analyses demonstrate that the Lagrangian reconstructions have larger dry biases when convection intensity increases in the western part of the ASM. Hence, it is likely the underestimated moistening effect of ice injection of region. These findings suggest that underestimated moistening from convection in the western region of the Asian monsoon which controls the dry bias of Lagrangian reconstructions in the ASM. Investigating similar connections between model dry biases and convective intensity in other regions appears promising for improving simulations of the UTLS moisture budget, part of the ASM is a key driver of the dry bias in the reconstructions.

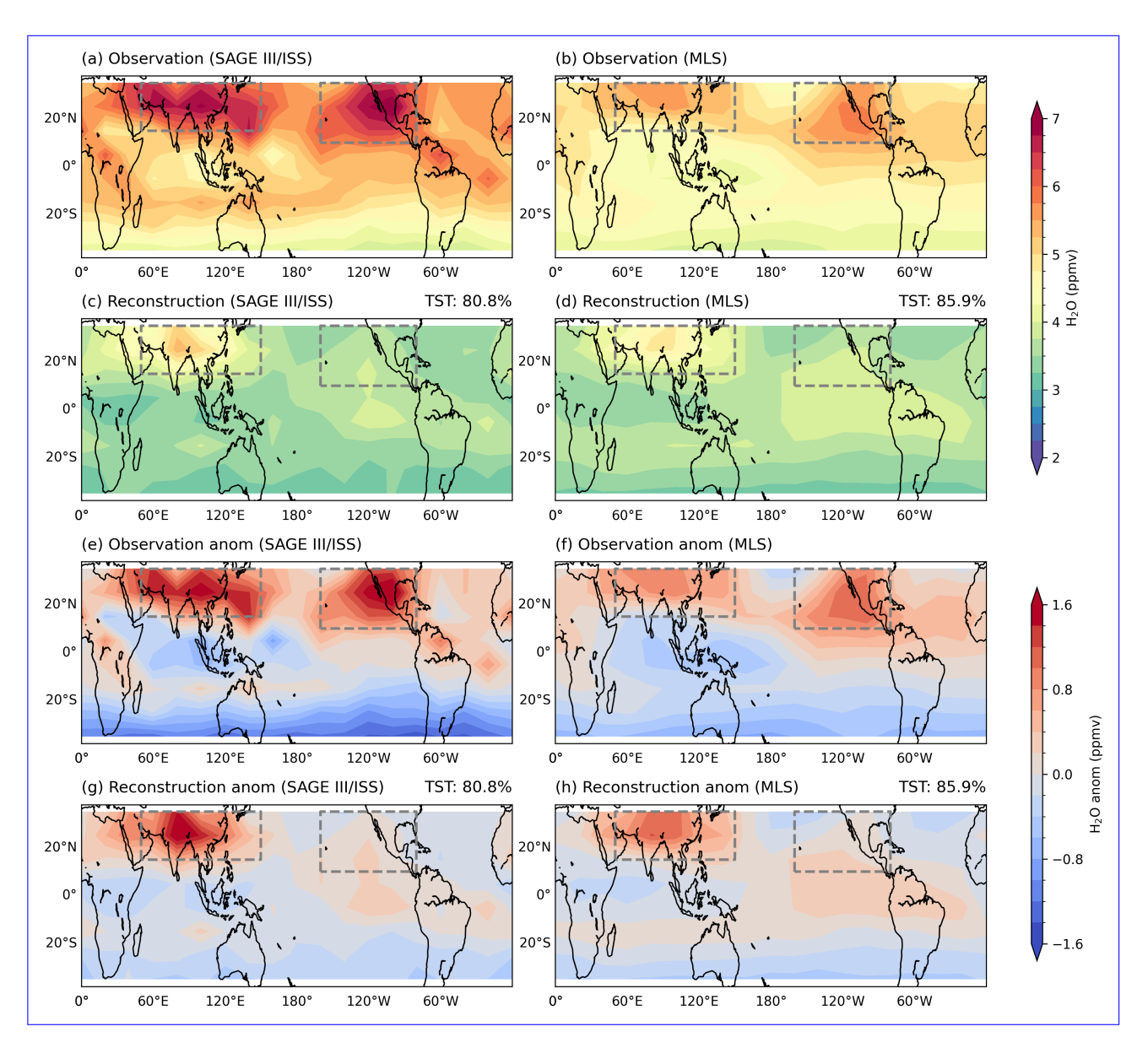


Figure 1. Horizontal distribution distributions of water vapor eoneentrations and anomalies in August. Observed water vapor (H₂O) concentrations mixing ratios and anomalies in August. Panels (a-b) show observed water vapor mixing ratios, the reconstructed concentrations of Experiment LAG (c-d) reconstructed mixing ratios from experiment LAG, and corresponding anomalies (e-h) the corresponding spatial anomalies, based on SAGE III/ISS (2017–2022) at 16.5 km (left) and MLS (2017–2019) at ~16.3 km (right). The anomalies are calculated by subtracting the average values of relative to the entire tropics tropical mean (35°S to 35S–35°N). Grey boxes in each subplot show indicate the defined area of ASM region (15°–35°N, 50°–150°E) and NAM region (10°–35°N, 160°–80°W). Reconstructions in this figure use include both TSTs TST and non-TSTs, non-TST trajectories; the portions fraction of TST are shown with TSTs is given in the upper right strings of panels (c-d) and (g-h).

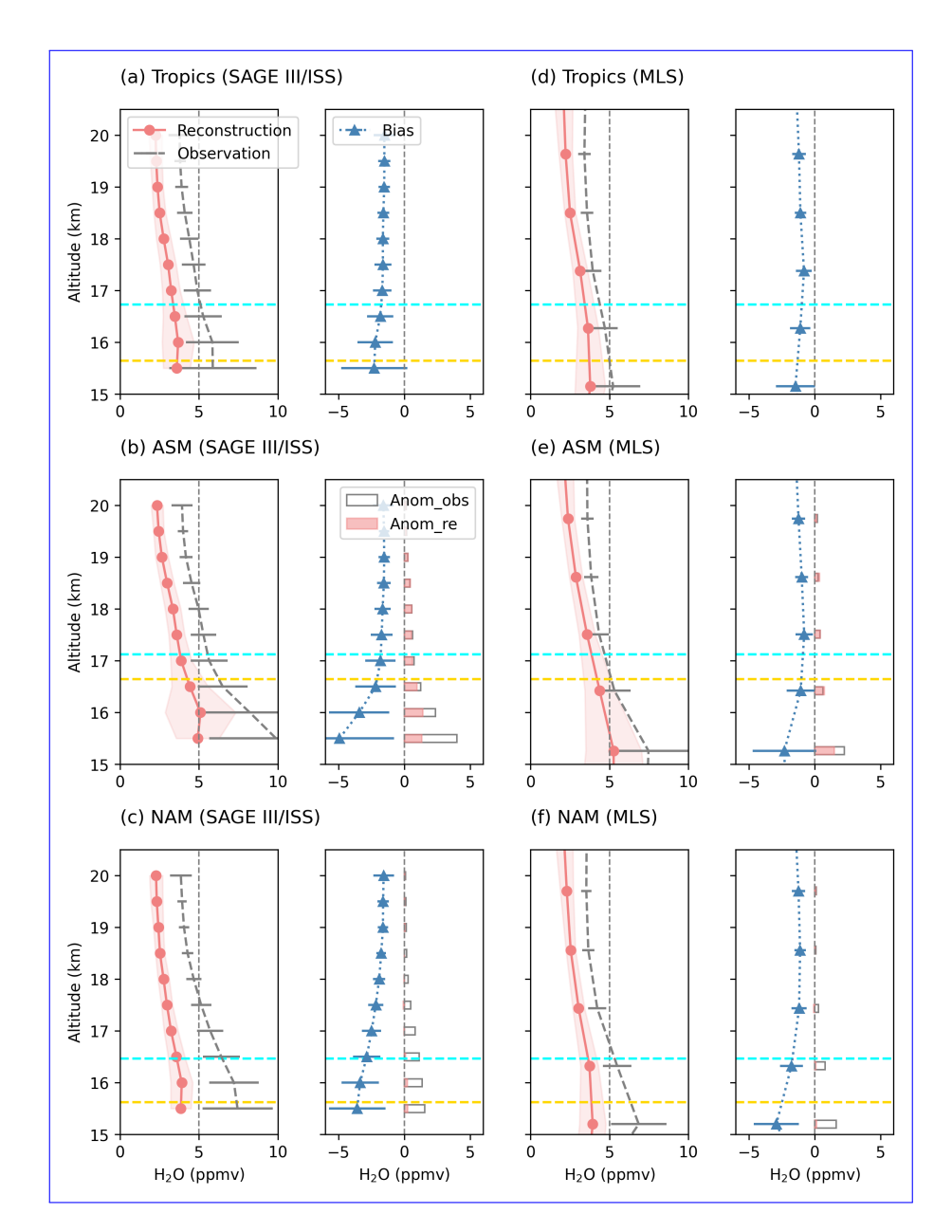


Figure 2. Vertical profiles of water vapor (H₂O) concentrations mixing ratios in August. For each subplot, it shows observed water vapor concentrations (grey Grey dotted lines) show observations, coral lines show reconstructed concentrations of Experiment values from experiment LAG (coral lines, TST-only), and the bias between them blue lines show reconstruction biases (reconstructed values subtract minus observed values, blue lines). Upper, middle and lower columns show Shading (or horizontal bars) indicates ±1 standard deviation around the respective profiles. Panels are averaged values in over the tropics (35°S-35°N; a, d), ASM (b, e), and NAM (c, from f), with results based on SAGE III/ISS (leftpanels) and MLS (rightpanels). The eyan horizontal Cyan dashed lines indicate the position of mark the climatological cold point tropopause in August, while the and yellow horizontal dashed lines represent mark the lapse rate tropopause defined by WMO. Both tropopauses are derived (both from ERA5reanalysis). For the In ASM and NAM panels (b, e) and NAM (; c, f), the gray grey bars in the right sub-panels represent the indicate observed anomalies, while the moisture enhancement and coral bars indicate the show reconstructed anomalies. The anomalies are calculated by subtracting the corresponding mean values in the tropics moisture enhancement, as shown relative to the tropical means in (a) and (d).

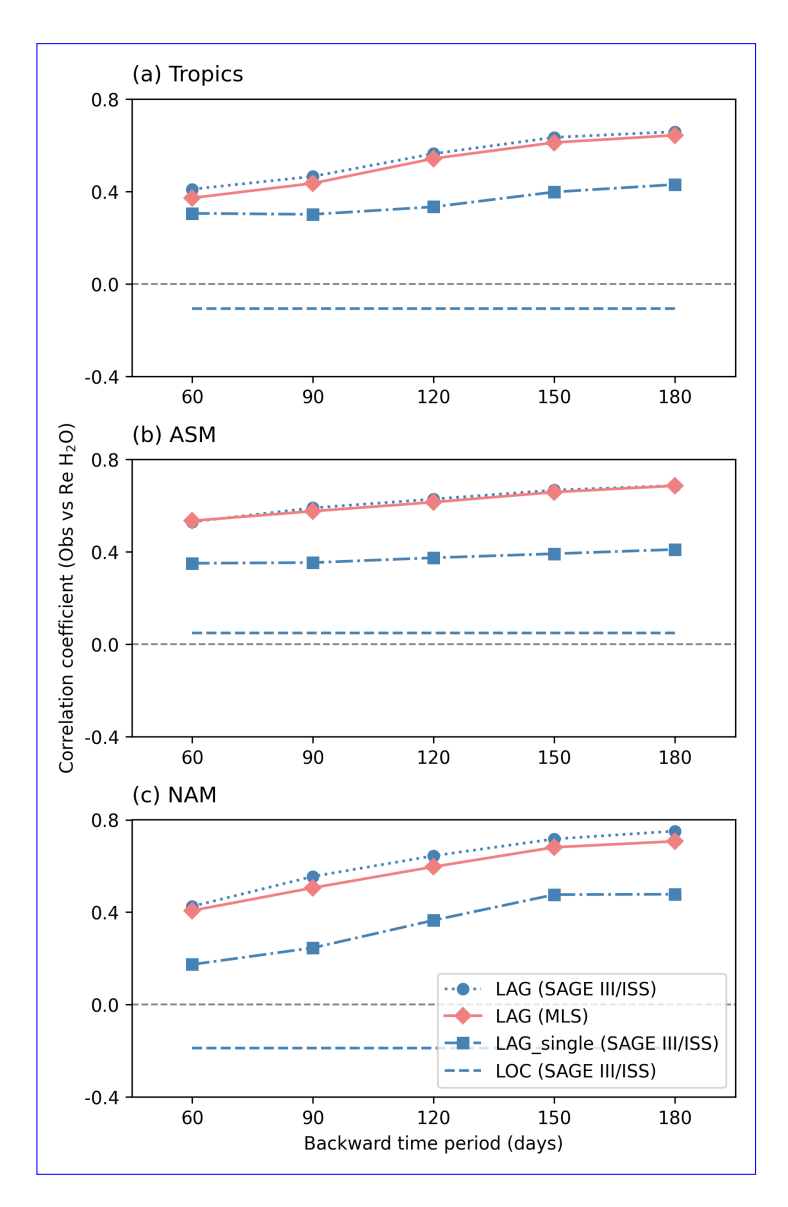


Figure 3. Correlation coefficients between observed and reconstructed water vapor concentrations mixing ratios (TST-only). Upper, middle and lower panels show the correlation coefficients between for all points within 15.5–20.0 kmwithin in entire. Panels show results for the tropics (a), ASM (b), and NAM (c), respectively. Red diamonds represent the indicate results of Experiment experiment LAG based on MLSdataset. Blue crosses, squares markers and rounds represent the lines indicate results based on SAGE III/ISSdataset of: dashed lines for LOC, squares for LAG_single, and circles for LAG, respectively. The LOC values remain constant as because they do not vary with depend on backward time in the Lagrangian experiments.

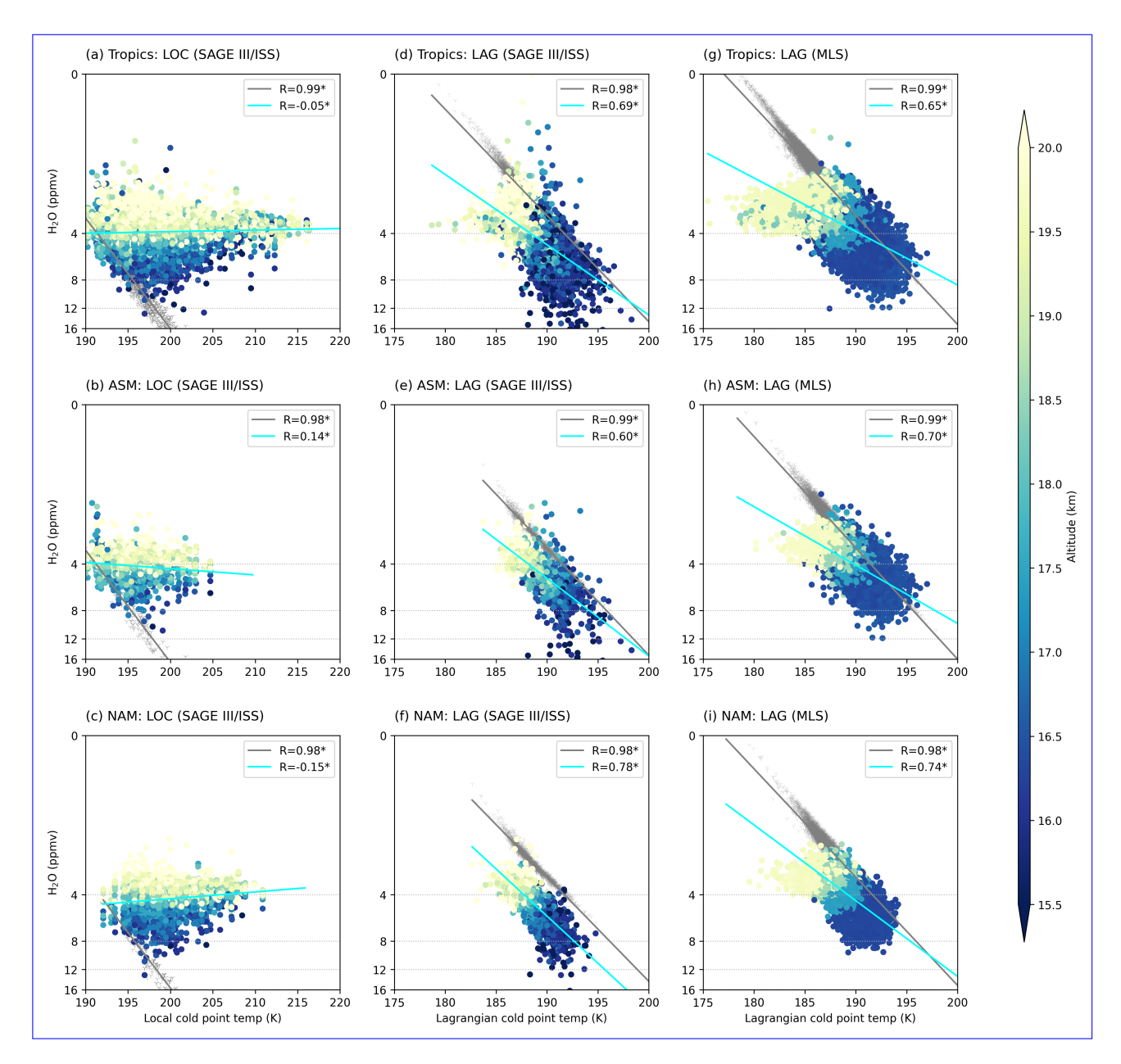


Figure 4. Scatters—Scatter plots of water vapor (H₂O) concentrations mixing ratios (TST-only) vs-versus cold point temperatures. Left: water vapor concentrations from observations (SAGE III/ISSvs-) water vapor versus local cold point temperatures (Experiment experiment LOC). Middle: water vapor concentrations from observations (SAGE III/ISSvs-) versus Lagrangian cold point temperatures (Experiment experiment LAG based on SAGE III/ISS). Right: water vapor concentrations from observations (MLSvs-) versus Lagrangian cold point temperatures (Experiment experiment LAG based on MLS). Coloured Colored points indicate the observed denote water vapor concentrations observations, with the colour showing altitudes of the pointscolor indicating altitude. Grey dots represent reconstructed concentrations (saturation)mixing ratios. The legends show Legends give the correlation coefficients and , with stars indicate marking statistical significance at the 95% confidence level based on the (Student's t-test).

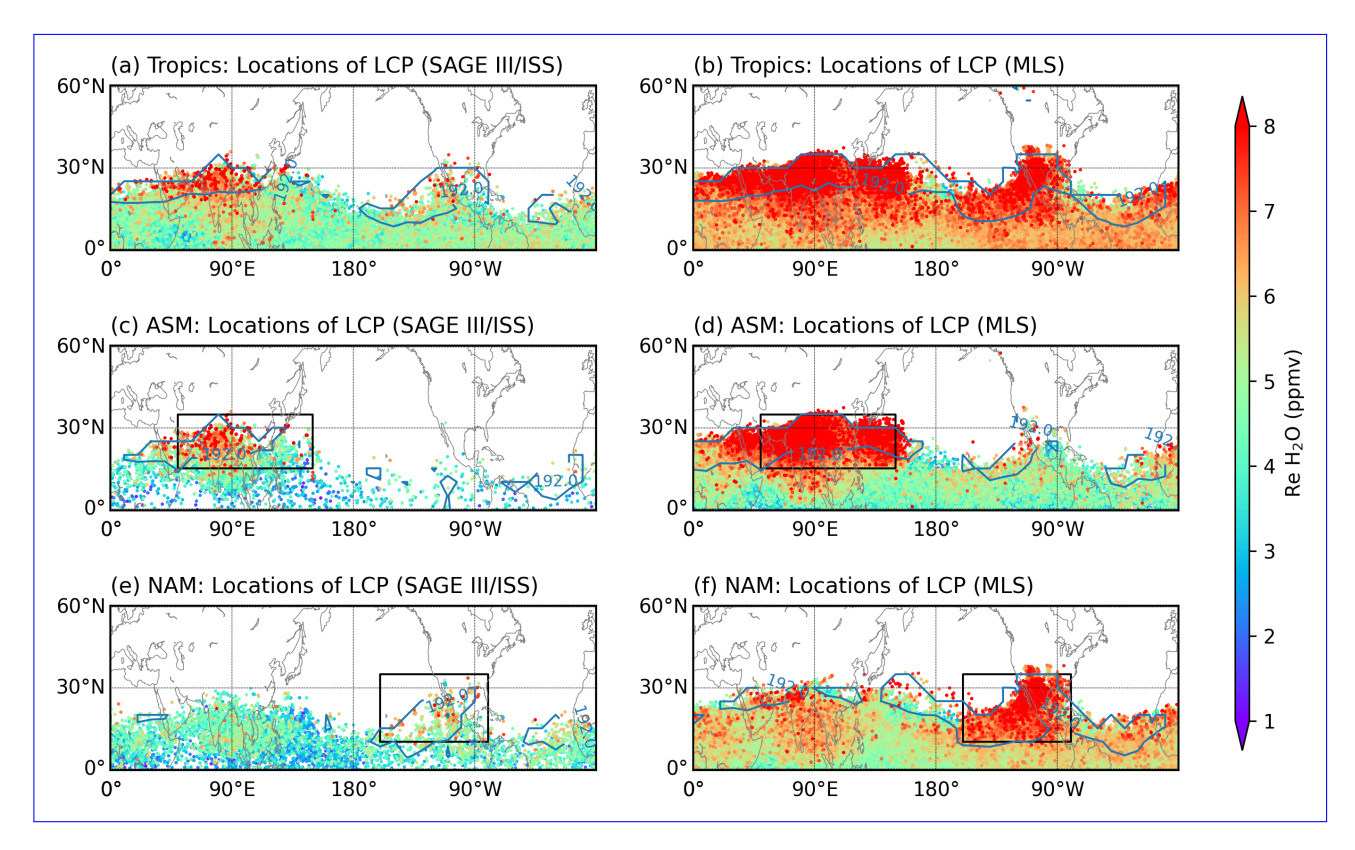


Figure 5. Horizontal distributions of the locations of the Lagrangian cold points point (LCPsLCP) locations used for water vapor (H₂O) reconstruction at 16.5 km, derived from Experiment experiment LAG (TST-only). The locations of the LCPs are shown with colors representing Colors denote the reconstructed water vapor concentrations mixing ratios (Re H₂O) at the LCPs, with starting points backward trajectories launched in the entire tropics (a, b), ASM (c, d), and NAM (e, f). The seatters Scatter points are plotted in ascending sequence according to the values order of reconstructions reconstructed values. The blue contour lines represent a cold point temperatures of Blue contours mark the 192 K cold point temperature. The left Left panels (a, c, e) show results based on SAGE III/ISS, while the and right panels (b, d, f) show results based on MLSdata. The black Black boxes indicate the original regions of starting points where the backward trajectories are launched.

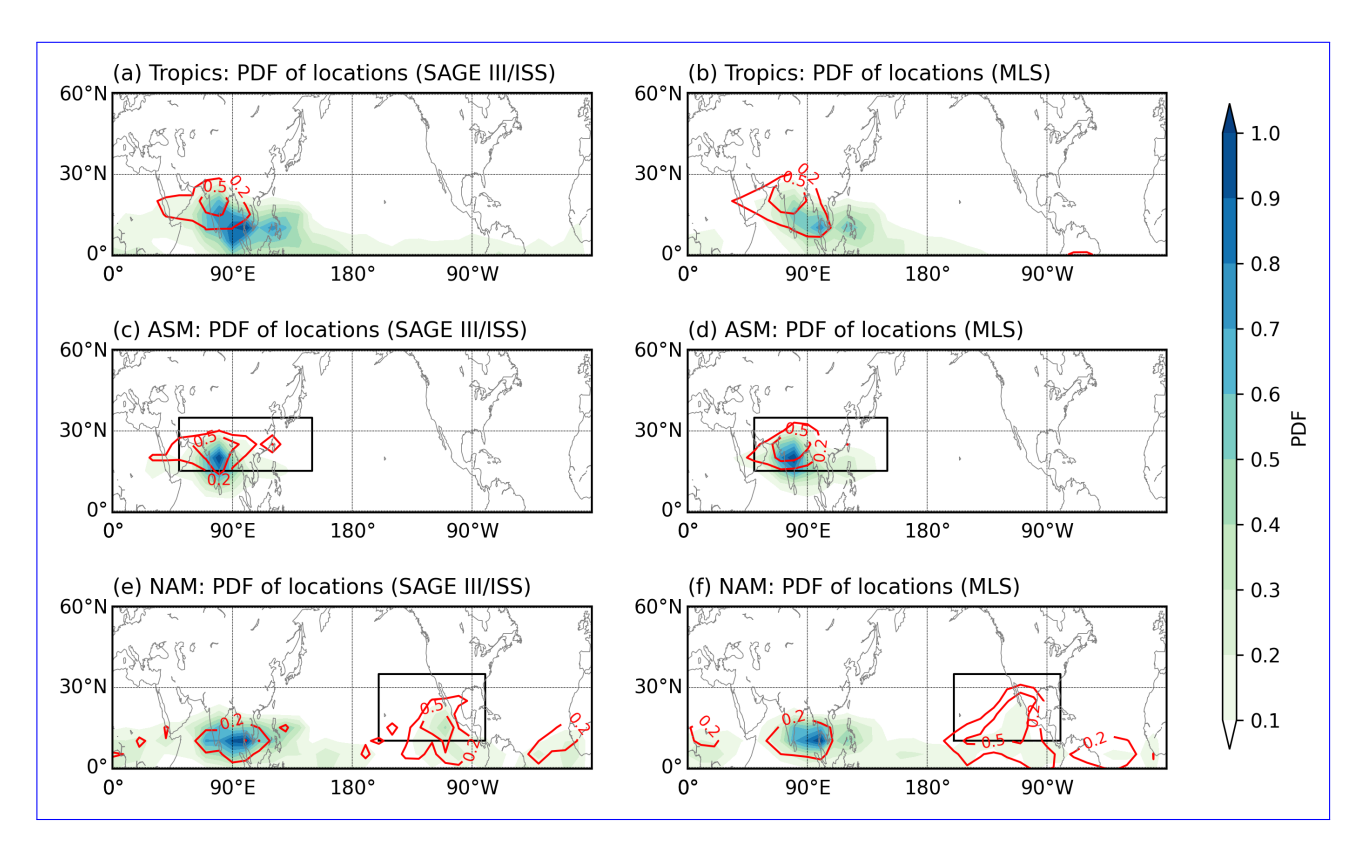


Figure 6. Probability density functions (PDFs) of the locations of Lagrangian cold points (LCPs) shown in Fig. 5. The PDFs Results are presented for the entire tropics (a, b), ASM (c, d), and NAM (e, f), with red. Red contour lines representing mark the PDFs of the locations with the top 10% highest of reconstructed water vapor concentrations mixing ratios. The left Left panels (a, c, e) show results based on SAGE III/ISS, while the and right panels (b, d, f) show results based on MLSdata.

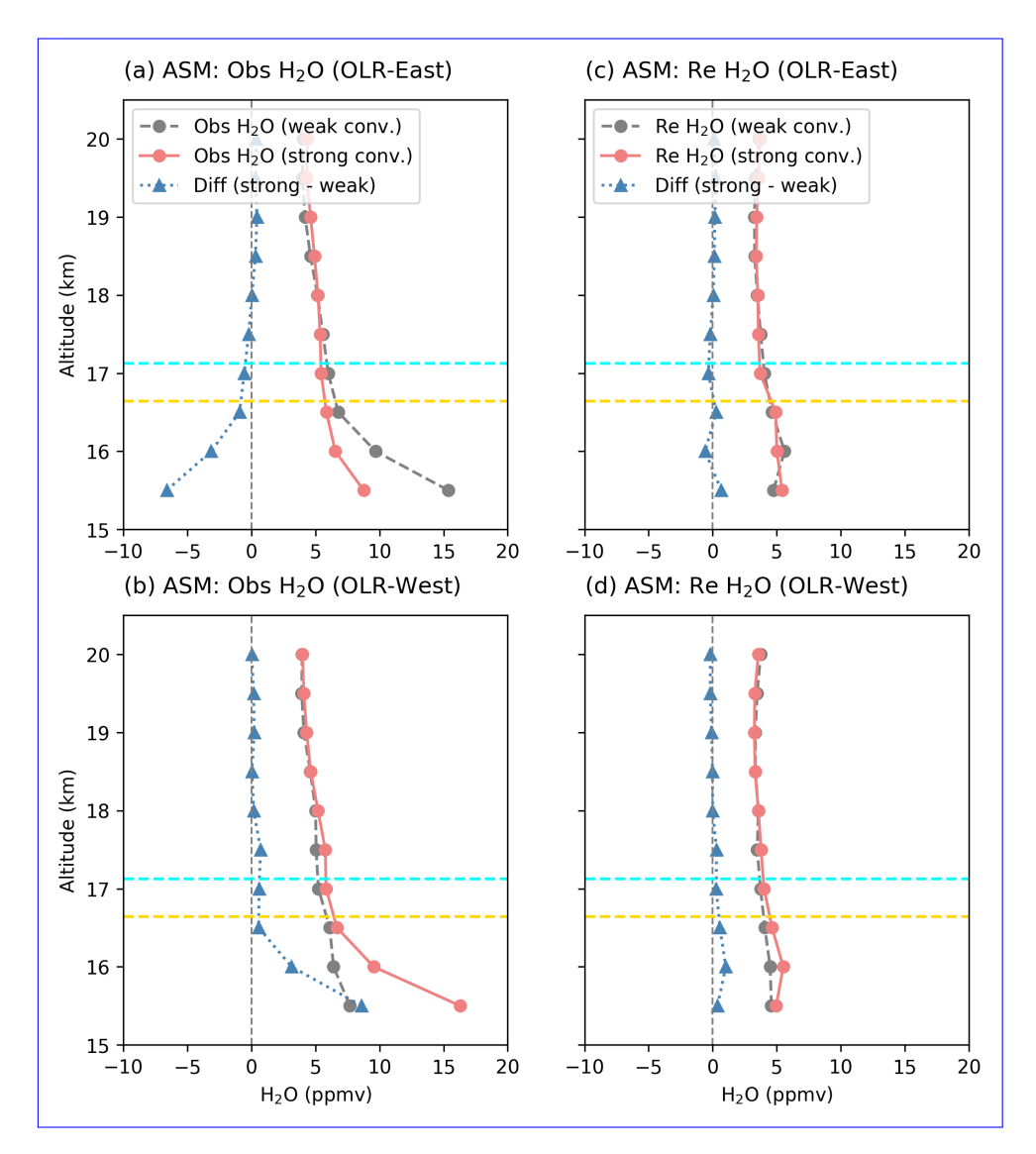


Figure 7. Vertical profiles of water vapor (H₂O) concentrations mixing ratios in the ASM region under the influence of convection within the ASM region, based on SAGE III/ISSdataset. The left-Left panels show observed water vapor-profiles averaged during over the 0–10 days following weak-convection (high-OLR grey lines) and strong-convection (low-OLR coral lines) days, along with their differences (blue lines), for OLR-West (a) and OLR-East (b) indices, where OLR is averaged over the western and eastern regions, respectively. Right panels show reconstructed water vapor profiles averaged during weak-convection days, for weak- and strong-convection days, and their differences, for OLR-West (c) and OLR-East (d)indices. Same as As in Fig.-2, the cyan and yellow horizontal dashed lines indicate the positions of mark the climatological cold point tropopause and lapse rate tropopauses in August, respectively.

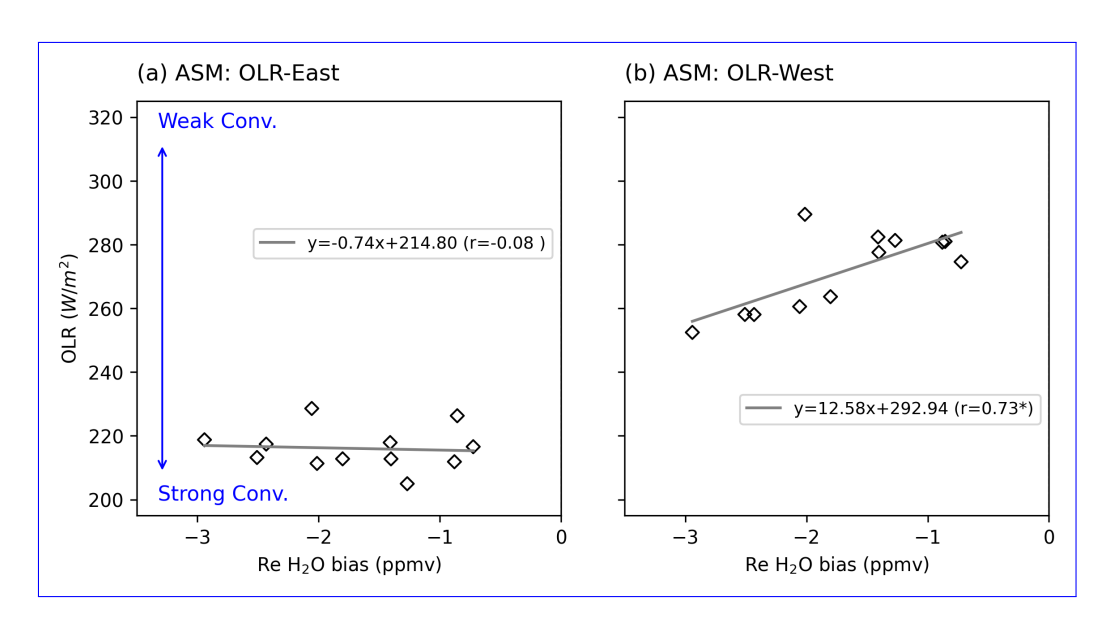


Figure 8. Scatter plots of OLR (convection intensity) versus biases in reconstructed water vapor concentrations (H₂O) mixing ratios (SAGE III/ISS) at 16.5 km for the ASM. Panels (a) and (b) correspond to show results using OLR-East and OLR-West, respectively. The biases Biases are half-monthly averaged averages, while OLR values are first averaged over the 0–10 days preceding each date and then half-monthly averaged. The legends display Legends show the regression line equations and correlation coefficients, with a star indicating statistical significance at the 95% confidence level based on the Student's t-test.

Code and data availability. The CLaMS model is available in the CLaMS git database. Detailed information is available at https://clams. icg.kfa-juelich.de/CLaMS/GitLabInstructions. ERA5 reanalysis data are available from the European Centre for Medium-range Weather Forecasts (https://apps.ecmwf.int/data-catalogues/era5/?class=ea), last access: 03 August 2024). The MLS v5.0 water vapor data used in this study are available from NASA's Earthdata website (https://www.earthdata.nasa.gov/learn/find-data/near-real-time/mls). SAGE III/ISS Level 2 Solar Event Species Profiles (HDF5) Version 5.3 data can be accessed through NASA's Atmospheric Science Data Center (https://asdc.larc.nasa.gov/project/SAGE%20III-ISS/g3bssp_53). The NOAA CPC OLR data are available at (https://psl.noaa.gov/data/gridded/data.cpc_blended_olr-2.5deg.html).

Author contributions. H. W. carried out the analysis and wrote the original draft of the manuscript. P. K. and F. P. supervised the research, contributing ideas, guidance, and discussions throughout the study, and assisted with iterative revisions. M. P., M. T., C. P., and N. P. provided comments and suggestions during the manuscript revision. All authors contributed to discussions and final revisions of the paper.

Competing interests. The authors declare no competing interests.

645 Acknowledgements. The authors would like to express their gratitude to the European Centre for Medium-Range Weather Forecasts (ECMWF) for providing meteorological analysis for this study. We extend our appreciation to Nicole Thomas for her exceptional programming support. Additionally, we thank ChatGPT (https://chat.openai.com, last accessed: March 2025) for their assistance in refining the final text. The CPC Daily Blended Outgoing Longwave Radiation (OLR) - 2.5 degree data was kindly provided by the NOAA PSL, Boulder, Colorado, USA, via their website at https://psl.noaa.gov. FP acknowledges support by the Deutsche Forschungsgemeinschaft (TPChange grant, The Tropopause Region in a Changing Atmosphere, DFG TRR 301, Project-ID 428312742).

References

660

- Avery, M., Davis, S., Rosenlof, K., Ye, H., and Dessler, A.: Large anomalies in lower stratospheric water vapour and ice during the 2015-2016 El Ninõ, Nature Geoscience, 10, 405–409, https://doi.org/10.1038/ngeo2961, cited By 67, 2017.
- Bannister, R., O'Neill, A., Gregory, A., and Nissen, K.: The role of the south-east Asian monsoon and other seasonal features in creating the 'tape-recorder' signal in the Unified Model, Quarterly Journal of the Royal Meteorological Society, 130, 1531 – 1554, https://doi.org/10.1256/qj.03.106, cited by: 63, 2004.
 - Bourguet, S. and Linz, M.: The impact of improved spatial and temporal resolution of reanalysis data on Lagrangian studies of the tropical tropopause layer, Atmospheric Chemistry and Physics, 22, 13 325–13 339, https://doi.org/10.5194/acp-22-13325-2022, cited By 6, 2022.
 - Brewer, A.: Evidence for a world circulation provided by the measurements of helium and water vapour distribution in the stratosphere, Quarterly Journal of the Royal Meteorological Society, 75, 351–363, https://doi.org/10.1002/qj.49707532603, cited By 831, 1949.
 - Cisewski, M., Zawodny, J., Gasbarre, J., Eckman, R., Topiwala, N., Rodriguez-Alvarez, O., Cheek, D., and Hall, S.: The stratospheric aerosol and gas experiment (SAGE III) on the International Space Station (ISS) Mission, in: Sensors, Systems, and Next-Generation Satellites XVIII, vol. 9241, pp. 59–65, SPIE, 2014.
- Clemens, J., Ploeger, F., Konopka, P., Portmann, R., Sprenger, M., and Wernli, H.: Characterization of transport from the Asian summer monsoon anticyclone into the UTLS via shedding of low potential vorticity cutoffs, Atmospheric Chemistry and Physics, 22, 3841 3860, https://doi.org/10.5194/acp-22-3841-2022, cited by: 3; All Open Access, Gold Open Access, Green Open Access, 2022.
 - Davis, S., Damadeo, R., Flittner, D., Rosenlof, K., Park, M., Randel, W., Hall, E., Huber, D., Hurst, D., Jordan, A., Kizer, S., Millan, L., Selkirk, H., Taha, G., Walker, K., and Vömel, H.: Validation of SAGE III/ISS Solar Water Vapor Data With Correlative Satellite and Balloon-Borne Measurements, Journal of Geophysical Research: Atmospheres, 126, https://doi.org/10.1029/2020JD033803, cited by: 11; All Open Access, Bronze Open Access, 2021.
 - Fu, R., Hu, Y., Wright, J. S., Jiang, J. H., Dickinson, R. E., Chen, M., Filipiak, M., Read, W. G., Waters, J. W., and Wu, D. L.: Short circuit of water vapor and polluted air to the global stratosphere by convective transport over the Tibetan Plateau, Proceedings of the National Academy of Sciences of the United States of America, 103, 5664 5669, https://doi.org/10.1073/pnas.0601584103, cited by: 268; All Open Access, Green Open Access, 2006.
- Fueglistaler, S. and Haynes, P.: Control of interannual and longer-term variability of stratospheric water vapor, Journal of Geophysical Research Atmospheres, 110, 1 14, https://doi.org/10.1029/2005JD006019, cited by: 161; All Open Access, Bronze Open Access, 2005.
 - Fueglistaler, S., Wernli, H., and Peter, T.: Tropical troposphere-to-stratosphere transport inferred from trajectory calculations, Journal of Geophysical Research: Atmospheres, 109, D03 108 1–16, https://doi.org/10.1029/2003jd004069, cited by: 162; All Open Access, Bronze Open Access, 2004.
- Fueglistaler, S., Bonazzola, M., Haynes, P. H., and Peter, T.: Stratospheric Water Vapor Predicted From the Lagrangian Temperature History of Air Entering the Stratosphere in the Tropics, Journal of Geophysical Research Atmospheres, https://doi.org/10.1029/2004jd005516, 2005.
 - Fueglistaler, S., Dessler, A., Dunkerton, T., Folkins, I., Fu, Q., and Mote, P.: Tropical tropopause layer, Reviews of Geophysics, 47, https://doi.org/10.1029/2008RG000267, cited by: 743; All Open Access, Bronze Open Access, 2009.
- Hasebe, F. and Noguchi, T.: A Lagrangian description on the troposphere-to-stratosphere transport changes associated with the stratospheric water drop around the year 2000, Atmospheric Chemistry and Physics, 16, 4235 4249, https://doi.org/10.5194/acp-16-4235-2016, cited by: 5; All Open Access, Gold Open Access, Green Open Access, 2016.

- Haynes, P. and Anglade, J.: The vertical-scale cascade in atmospheric tracers due to large-scale differential advection, Journal of the Atmospheric Sciences, 54, 1121 1136, https://doi.org/10.1175/1520-0469(1997)054<1121:TVSCIA>2.0.CO;2, cited by: 125; All Open Access, Bronze Open Access, 1997.
 - Hersbach, H., Bell, B., Berrisford, P., Hirahara, S., Horányi, A., Muñoz-Sabater, J., Nicolas, J., Peubey, C., Radu, R., Schepers, D., Simmons, A., Soci, C., Abdalla, S., Abellan, X., Balsamo, G., Bechtold, P., Biavati, G., Bidlot, J., Bonavita, M., De Chiara, G., Dahlgren, P., Dee, D., Diamantakis, M., Dragani, R., Flemming, J., Forbes, R., Fuentes, M., Geer, A., Haimberger, L., Healy, S., Hogan, R. J., Hólm, E., Janisková, M., Keeley, S., Laloyaux, P., Lopez, P., Lupu, C., Radnoti, G., de Rosnay, P., Rozum, I., Vamborg, F., Villaume, S., and Thépaut, J.-N.: The ERA5 global reanalysis, Quarterly Journal of the Royal Meteorological Society, 146, 1999 2049, https://doi.org/10.1002/qi.3803, cited by: 11844; All Open Access, Hybrid Gold Open Access, 2020.

720

- Holton, J. R. and Gettelman, A.: Horizontal transport and the dehydration of the stratosphere, Geophysical Research Letters, 28, 2799 2802, https://doi.org/10.1029/2001GL013148, cited by: 318, 2001.
- Homeyer, C. R., Smith, J. B., Bedka, K. M., Bowman, K. P., Wilmouth, D. M., Ueyama, R., Dean-Day, J. M., St. Clair, J. M., Hannun,
 R., Hare, J., et al.: Extreme altitudes of stratospheric hydration by midlatitude convection observed during the DCOTSS field campaign,
 Geophysical Research Letters, 50, e2023GL104 914, 2023.
 - Homeyer, C. R., Gordon, A. E., Smith, J. B., Ueyama, R., Wilmouth, D. M., Sayres, D. S., Hare, J., Pandey, A., Hanisco, T. F., Dean-Day, J. M., et al.: Stratospheric hydration processes in tropopause-overshooting convection revealed by tracer-tracer correlations from the DCOTSS field campaign, Journal of Geophysical Research: Atmospheres, 129, e2024JD041 340, 2024.
- Honomichl, S. B. and Pan, L. L.: Transport From the Asian Summer Monsoon Anticyclone Over the Western Pacific, Journal of Geophysical Research: Atmospheres, 125, https://doi.org/10.1029/2019JD032094, cited by: 27, 2020.
 - James, R., Bonazzola, M., Legras, B., Surbled, K., and Fueglistaler, S. A.: Water vapor transport and dehydration above convective outflow during Asian monsoon, Geophysical Research Letters, 35, https://doi.org/10.1029/2008GL035441, cited by: 94; All Open Access; Bronze Open Access, 2008.
- Jensen, E., Pan, L., Honomichl, S., Diskin, G., Krämer, M., Spelten, N., Günther, G., Hurst, D., Fujiwara, M., Vömel, H., Selkirk, H., Suzuki, J., Schwartz, M., and Smith, J.: Assessment of Observational Evidence for Direct Convective Hydration of the Lower Stratosphere, Journal of Geophysical Research: Atmospheres, 125, https://doi.org/10.1029/2020JD032793, cited By 20, 2020.
 - Jorgensen, D. and Lemone, M.: Vertical velocity characteristics of oceanic convection, Journal of the Atmospheric Sciences, 46, 621 640, https://doi.org/10.1175/1520-0469(1989)046<0621:VVCOOC>2.0.CO;2, cited by: 201; All Open Access, Bronze Open Access, 1989.
- 715 Konopka, P., Tao, M., Von Hobe, M., Hoffmann, L., Kloss, C., Ravegnani, F., Volk, C. M., Lauther, V., Zahn, A., Hoor, P., and Ploeger, F.: Tropospheric transport and unresolved convection: numerical experiments with CLaMS 2.0/MESSy, Geoscientific Model Development, 15, 7471 7487, https://doi.org/10.5194/gmd-15-7471-2022, cited by: 5; All Open Access, Gold Open Access, Green Open Access, 2022.
 - Konopka, P., Rolf, C., Von Hobe, M., Khaykin, S. M., Clouser, B., Moyer, E., Ravegnani, F., D'Amato, F., Viciani, S., Spelten, N., Afchine, A., Krämer, M., Stroh, F., and Ploeger, F.: The dehydration carousel of stratospheric water vapor in the Asian summer monsoon anticyclone, Atmospheric Chemistry and Physics, 23, 12 935 12 947, https://doi.org/10.5194/acp-23-12935-2023, 2023.
 - Kumar, V. and Krishnan, R.: On the association between the Indian summer monsoon and the tropical cyclone activity over northwest Pacific, Current science, pp. 602–612, 2005.
 - Lambert, A., Werner, F., Read, W. G., Froidevaux, L., Schwartz, M. J., Wagner, P. A., Daffer, W. H., Livesey, N. J., Pumphrey, H. C., Manney, G. L., et al.: Version 5 Level-2 Near-Real-Time Data User Guide, Tech. rep., Tech. Rep. JPL D-48439 d, Jet Propulsion Laboratory, California Institute of ..., 2017.

- Liu, C., Zipser, E. J., and Nesbitt, S. W.: Global distribution of tropical deep convection: Different perspectives from TRMM infrared and radar data, Journal of Climate, 20, 489 503, https://doi.org/10.1175/JCLI4023.1, cited by: 190; All Open Access, Bronze Open Access, Green Open Access, 2007.
- Liu, Y., Fueglistaler, S., and Haynes, P.: Advection-condensation paradigm for stratospheric water vapor, Journal of Geophysical Research
 Atmospheres, 115, https://doi.org/10.1029/2010JD014352, cited by: 62, 2010.
 - Livesey, N., Read, W., Wagner, L., Froidevaux, P., Lambert, A., Manney, G., Millán Valle, L., Pumphrey, H., Santee, M., Schwartz, M., et al.: Version 4.2 x Level 2 and 3 data quality and description document (Tech. Rep. No. JPL D-33509 Rev. E), Jet Propulsion Laboratory, 2020.
 - McKenna, D. S., Grooß, J.-U., Günther, G., Konopka, P., Müller, R., Carver, G., and Sasano, Y.: A new Chemical Lagrangian Model of the Stratosphere (CLaMS) 2. Formulation of chemistry scheme and initialization, Journal of Geophysical Research Atmospheres, 107, ACH 4–1 ACH 4–14, https://doi.org/10.1029/2000JD000113, cited by: 116, 2002.

- Mote, P. W., Rosenlof, K. H., Holton, J. R., Harwood, R. S., and Waters, J. W.: Seasonal variations of water vapor in the tropical lower stratosphere, Geophysical Research Letters, 22, 1093 1096, https://doi.org/10.1029/95GL01234, cited by: 83, 1995.
- Mote, P. W., Rosenlof, K. H., McIntyre, M. E., Carr, E. S., Gille, J. C., Holton, J. R., Kinnersley, J. S., Pumphrey, H. C., Russell III, J. M., and Waters, J. W.: An atmospheric tape recorder: The imprint of tropical tropopause temperatures on stratospheric water vapor, Journal of Geophysical Research Atmospheres, 101, 3989 4006, https://doi.org/10.1029/95JD03422, cited by: 626; All Open Access, Green Open Access, 1996.
- Nützel, M., Podglajen, A., Garny, H., and Ploeger, F.: Quantification of water vapour transport from the Asian monsoon to the stratosphere, Atmospheric Chemistry and Physics, 19, 8947 8966, https://doi.org/10.5194/acp-19-8947-2019, cited by: 22; All Open Access, Gold Open Access, 2019.
- O'Neill, M., Orf, L., Heymsfield, G., and Halbert, K.: Hydraulic jump dynamics above supercell thunderstorms, Science, 373, 1248–1251, https://doi.org/10.1126/science.abh3857, cited By 24, 2021.
 - Park, M., Randel, W. J., Gettelman, A., Massie, S. T., and Jiang, J. H.: Transport above the Asian summer monsoon anticyclone inferred from Aura Microwave Limb Sounder tracers, Journal of Geophysical Research Atmospheres, 112, https://doi.org/10.1029/2006JD008294, cited by: 280; All Open Access, Bronze Open Access, Green Open Access, 2007.
- Park, M., Randel, W. J., Damadeo, R. P., Flittner, D. E., Davis, S. M., Rosenlof, K. H., Livesey, N., Lambert, A., and Read, W.: Near-Global Variability of Stratospheric Water Vapor Observed by SAGE III/ISS, Journal of Geophysical Research: Atmospheres, 126, https://doi.org/10.1029/2020JD034274, cited by: 6; All Open Access, Green Open Access, 2021.
 - Peña-Ortiz, C., Plaza, N. P., Gallego, D., and Ploeger, F.: Quasi-biennial oscillation modulation of stratospheric water vapour in the Asian monsoon, Atmospheric Chemistry and Physics, 24, 5457 5478, https://doi.org/10.5194/acp-24-5457-2024, cited by: 0, 2024.
- Pierrehumbert, R. T. and Roca, R.: Evidence for control of atlantic subtropical humidity by large scale advection, Geophysical Research Letters, 25, 4537 4540, https://doi.org/10.1029/1998GL900203, cited by: 114; All Open Access; Green Accepted Open Access; Green Open Access, 1998.
 - Pisso, I., Marécal, V., Legras, B., and Berthet, G.: Sensitivity of ensemble Lagrangian reconstructions to assimilated wind time step resolution, Atmospheric Chemistry and Physics, 10, 3155–3162, https://doi.org/10.5194/acp-10-3155-2010, cited By 11, 2010.
- Plaza, N. P., Podglajen, A., Peña-Ortiz, C., and Ploeger, F.: Processes influencing lower stratospheric water vapour in monsoon anticyclones: insights from Lagrangian modelling, Atmospheric Chemistry and Physics, 21, 9585–9607, 2021.

- Ploeger, F., Fueglistaler, S., Grooß, J.-U., Günther, G., Konopka, P., Liu, Y., Uller, R., Ravegnani, F., Schiller, C., Ulanovski, A., and Riese, M.: Insight from ozone and water vapour on transport in the tropical tropopause layer (TTL), Atmospheric Chemistry and Physics, 11, 407–419, https://doi.org/10.5194/acp-11-407-2011, cited By 54, 2011.
- Ploeger, F., Günther, G., Konopka, P., Fueglistaler, S., Müller, R., Hoppe, C., Kunz, A., Spang, R., Grooß, J.-U., and Riese, M.: Horizontal water vapor transport in the lower stratosphere from subtropics to high latitudes during boreal summer, Journal of Geophysical Research Atmospheres, 118, 8111 8127, https://doi.org/10.1002/jgrd.50636, cited by: 98; All Open Access, Green Open Access, 2013.

775

785

- Poshyvailo, L., Müller, R., Konopka, P., Günther, G., Riese, M., Podglajen, A., and Ploeger, F.: Sensitivities of modelled water vapour in the lower stratosphere: Temperature uncertainty, effects of horizontal transport and small-scale mixing, Atmospheric Chemistry and Physics, 18, 8505–8527, https://doi.org/10.5194/acp-18-8505-2018, cited By 18, 2018.
- Randel, W. and Park, M.: Diagnosing Observed Stratospheric Water Vapor Relationships to the Cold Point Tropical Tropopause, Journal of Geophysical Research: Atmospheres, 124, 7018–7033, https://doi.org/10.1029/2019JD030648, cited By 50, 2019.
- Randel, W., Moyer, E., Park, M., Jensen, E., Bernath, P., Walker, K., and Boone, C.: Global variations of HDO and HDO/H2O ratios in the upper troposphere and lower stratosphere derived from ACE-FTS satellite measurements, Journal of Geophysical Research Atmospheres, 117, https://doi.org/10.1029/2011JD016632, cited By 69, 2012.
- Randel, W. J., Wu, F., Oltmans, S. J., Rosenlof, K., and Nedoluha, G. E.: Interannual changes of stratospheric water vapor and correlations with tropical tropopause temperatures, Journal of the Atmospheric Sciences, 61, 2133 2148, https://doi.org/10.1175/1520-0469(2004)061<2133:ICOSWV>2.0.CO;2, cited by: 216; All Open Access, Bronze Open Access, 2004.
- Randel, W. J., Zhang, K., and Fu, R.: What controls stratospheric water vapor in the NH summer monsoon regions?, JOURNAL OF GEO-PHYSICAL RESEARCH-ATMOSPHERES, 120, 7988–8001, https://doi.org/10.1002/2015JD023622, 2015.
 - Read, W., Lambert, A., Bacmeister, J., Cofield, R., Christensen, L., Cuddy, D., Daffer, W., Drouin, B., Fetzer, E., Froidevaux, L., Fuller, R., Herman, R., Jarnot, R., Jiang, J., Jiang, Y., Kelly, K., Knosp, B., Kovalenko, L., Livesey, N., Liu, H.-C., Manney, G., Pickett, H., Pumphrey, H., Rosenlof, K. H., Sabounchi, X., Santee, M., Schwartz, M., Snyder, W., Stek, P., Su, H., Takacs, L., Thurstans, R., Vömel, H., Wagner, P., Waters, J., Webster, C., Weinstock, E., and Wu, D.: Aura Microwave Limb Sounder upper tropospheric and lower stratospheric H2O and relative humidity with respect to ice validation, Journal of Geophysical Research Atmospheres, 112, https://doi.org/10.1029/2007JD008752, cited by: 193; All Open Access, Bronze Open Access, 2007.
 - Riese, M., Ploeger, F., Rap, A., Vogel, B., Konopka, P., Dameris, M., and Forster, P.: Impact of uncertainties in atmospheric mixing on simulated UTLS composition and related radiative effects, JOURNAL OF GEOPHYSICAL RESEARCH-ATMOSPHERES, 117, https://doi.org/10.1029/2012JD017751, 2012.
- Rolf, C., Vogel, B., Hoor, P., Afchine, A., Günther, G., Krämer, M., Müller, R., Müller, S., Spelten, N., and Riese, M.: Water vapor increase in the lower stratosphere of the Northern Hemisphere due to the Asian monsoon anticyclone observed during the TACTS/ESMVal campaigns, Atmospheric Chemistry and Physics, 18, 2973 2983, https://doi.org/10.5194/acp-18-2973-2018, cited by: 23; All Open Access, Gold Open Access, 2018.
 - Schiller, C., Groob, J.-U., Konopka, P., Plöger, F., Silva Dos Santos, F., and Spelten, N.: Hydration and dehydration at the tropical tropopause, Atmospheric Chemistry and Physics, 9, 9647–9660, https://doi.org/10.5194/acp-9-9647-2009, cited By 73, 2009.
 - Schoeberl, M. and Dessler, A.: Dehydration of the stratosphere, Atmospheric Chemistry and Physics, 11, 8433 8446, https://doi.org/10.5194/acp-11-8433-2011, cited by: 92; All Open Access, Gold Open Access, Green Open Access, 2011.
 - Schoeberl, M. R., Dessler, A. E., and Wang, T.: Modeling upper tropospheric and lower stratospheric water vapor anomalies, Atmospheric Chemistry and Physics, 13, 7783–7793, https://doi.org/10.5194/acp-13-7783-2013, 2013.

- Schwartz, M. J., Read, W. G., Santee, M. L., Livesey, N. J., Froidevaux, L., Lambert, A., and Manney, G. L.: Convectively injected water vapor in the North American summer lowermost stratosphere, Geophysical Research Letters, 40, 2316 2321, https://doi.org/10.1002/grl.50421, cited by: 70; All Open Access, Bronze Open Access, 2013.
 - Smith, J., Wilmouth, D., Bedka, K., Bowman, K., Homeyer, C., Dykema, J., Sargent, M., Clapp, C., Leroy, S., Sayres, D., Dean-Day, J., Paul Bui, T., and Anderson, J.: A case study of convectively sourced water vapor observed in the overworld stratosphere over the United States, Journal of Geophysical Research: Atmospheres, 122, 9529–9554, https://doi.org/10.1002/2017JD026831, cited By 64, 2017.
 - Smith, J., Haynes, P., Maycock, A., Butchart, N., and Bushell, A.: Sensitivity of stratospheric water vapour to variability in tropical tropopause temperatures and large-scale transport, Atmospheric Chemistry and Physics, 21, 2469–2489, https://doi.org/10.5194/acp-21-2469-2021, cited By 7, 2021.
- Solomon, S., Rosenlof, K. H., Portmann, R. W., Daniel, J. S., Davis, S. M., Sanford, T. J., and Plattner, G.-K.: Contributions of Stratospheric Water Vapor to Decadal Changes in the Rate of Global Warming, SCIENCE, 327, 1219–1223, https://doi.org/10.1126/science.1182488, 2010.
 - Sonntag, D.: Advancements in the field of hygrometry, Meteorologische Zeitschrift, 3, 51–66, https://doi.org/10.1127/metz/3/1994/51, 1994. Tao, M., Konopka, P., Wright, J. S., Liu, Y., Bian, J., Davis, S. M., Jia, Y., and Ploeger, F.: Multi-decadal variability controls short-term stratospheric water vapor trends, Communications Earth and Environment, 4, https://doi.org/10.1038/s43247-023-01094-9, cited by: 2;
- All Open Access, Gold Open Access, 2023.

- Ueyama, R., Jensen, E., Pfister, L., Krämer, M., Afchine, A., and Schoeberl, M.: Impact of Convectively Detrained Ice Crystals on the Humidity of the Tropical Tropopause Layer in Boreal Winter, Journal of Geophysical Research: Atmospheres, 125, https://doi.org/10.1029/2020JD032894, cited By 9, 2020.
- Ueyama, R., Schoeberl, M., Jensen, E., Pfister, L., Park, M., and Ryoo, J.-M.: Convective Impact on the Global Lower Stratospheric Water Vapor Budget, Journal of Geophysical Research: Atmospheres, 128, https://doi.org/10.1029/2022JD037135, cited By 8, 2023.
 - Uma, K. N., Das, S. K., and Das, S. S.: A climatological perspective of water vapor at the UTLS region over different global monsoon regions: Observations inferred from the Aura-MLS and reanalysis data, Climate Dynamics, 43, 407 420, https://doi.org/10.1007/s00382-014-2085-9, cited by: 37, 2014.
- Vogel, B., Müller, R., Günther, G., Spang, R., Hanumanthu, S., Li, D., Riese, M., and Stiller, G.: Lagrangian simulations of the transport of young air masses to the top of the Asian monsoon anticyclone and into the tropical pipe, Atmospheric Chemistry and Physics, 19, 6007–6034, https://doi.org/10.5194/acp-19-6007-2019, cited By 64, 2019.
 - Waters, J. W., Froidevaux, L., Harwood, R. S., Jarnot, R. F., Pickett, H. M., Read, W. G., Siegel, P. H., Cofield, R. E., Filipiak, M. J., Flower, D. A., et al.: The earth observing system microwave limb sounder (EOS MLS) on the Aura satellite, IEEE transactions on geoscience and remote sensing, 44, 1075–1092, 2006.
- Wright, C. and Gille, J.: HIRDLS observations of gravity wave momentum fluxes over the monsoon regions, Journal of Geophysical Research Atmospheres, 116, https://doi.org/10.1029/2011JD015725, cited by: 35, 2011.
 - Yu, W., Dessler, A. E., Park, M., and Jensen, E. J.: Influence of convection on stratospheric water vapor in the North American monsoon region, Atmospheric Chemistry and Physics, 20, 12153 12161, https://doi.org/10.5194/acp-20-12153-2020, cited by: 12; All Open Access, Gold Open Access, Green Open Access, 2020.

835 References

840

850

- Avery, M., Davis, S., Rosenlof, K., Ye, H., and Dessler, A.: Large anomalies in lower stratospheric water vapour and ice during the 2015-2016 El Ninõ, Nature Geoscience, 10, 405–409, https://doi.org/10.1038/ngeo2961, cited By 67, 2017.
- Bannister, R., O'Neill, A., Gregory, A., and Nissen, K.: The role of the south-east Asian monsoon and other seasonal features in creating the 'tape-recorder' signal in the Unified Model, Quarterly Journal of the Royal Meteorological Society, 130, 1531 1554, , cited by: 63, 2004.
- Bourguet, S. and Linz, M.: The impact of improved spatial and temporal resolution of reanalysis data on Lagrangian studies of the tropical tropopause layer, Atmospheric Chemistry and Physics, 22, 13 325–13 339, https://doi.org/10.5194/acp-22-13325-2022, cited By 6, 2022.
- Brewer, A.: Evidence for a world circulation provided by the measurements of helium and water vapour distribution in the stratosphere, Quarterly Journal of the Royal Meteorological Society, 75, 351–363, https://doi.org/10.1002/qj.49707532603, cited By 831, 1949.
- Cisewski, M., Zawodny, J., Gasbarre, J., Eckman, R., Topiwala, N., Rodriguez-Alvarez, O., Cheek, D., and Hall, S.: The stratospheric aerosol and gas experiment (SAGE III) on the International Space Station (ISS) Mission, in: Sensors, Systems, and Next-Generation Satellites XVIII, vol. 9241, pp. 59–65, SPIE, 2014.
 - Clemens, J., Ploeger, F., Konopka, P., Portmann, R., Sprenger, M., and Wernli, H.: Characterization of transport from the Asian summer monsoon anticyclone into the UTLS via shedding of low potential vorticity cutoffs, Atmospheric Chemistry and Physics, 22, 3841 3860, https://doi.org/10.5194/acp-22-3841-2022, cited by: 3; All Open Access, Gold Open Access, Green Open Access, 2022.
 - Davis, S., Damadeo, R., Flittner, D., Rosenlof, K., Park, M., Randel, W., Hall, E., Huber, D., Hurst, D., Jordan, A., Kizer, S., Millan, L., Selkirk, H., Taha, G., Walker, K., and Vömel, H.: Validation of SAGE III/ISS Solar Water Vapor Data With Correlative Satellite and Balloon-Borne Measurements, Journal of Geophysical Research: Atmospheres, 126, https://doi.org/10.1029/2020JD033803, cited by: 11; All Open Access, Bronze Open Access, 2021.
- Fu, R., Hu, Y., Wright, J. S., Jiang, J. H., Dickinson, R. E., Chen, M., Filipiak, M., Read, W. G., Waters, J. W., and Wu, D. L.: Short circuit of water vapor and polluted air to the global stratosphere by convective transport over the Tibetan Plateau, Proceedings of the National Academy of Sciences of the United States of America, 103, 5664 5669, https://doi.org/10.1073/pnas.0601584103, cited by: 268; All Open Access, Green Open Access, 2006.
 - Fueglistaler, S. and Haynes, P.: Control of interannual and longer-term variability of stratospheric water vapor, Journal of Geophysical Research Atmospheres, 110, 1 14, https://doi.org/10.1029/2005JD006019, cited by: 161; All Open Access, Bronze Open Access, 2005.
 - Fueglistaler, S., Wernli, H., and Peter, T.: Tropical troposphere-to-stratosphere transport inferred from trajectory calculations, Journal of Geophysical Research: Atmospheres, 109, D03 108 1–16, https://doi.org/10.1029/2003jd004069, cited by: 162; All Open Access, Bronze Open Access, 2004.
- Fueglistaler, S., Bonazzola, M., Haynes, P. H., and Peter, T.: Stratospheric Water Vapor Predicted From the Lagrangian Temperature History of Air Entering the Stratosphere in the Tropics, Journal of Geophysical Research Atmospheres, https://doi.org/10.1029/2004jd005516, 2005.
 - Fueglistaler, S., Dessler, A., Dunkerton, T., Folkins, I., Fu, Q., and Mote, P.: Tropical tropopause layer, Reviews of Geophysics, 47, https://doi.org/10.1029/2008RG000267, cited by: 743; All Open Access, Bronze Open Access, 2009.
- Hasebe, F. and Noguchi, T.: A Lagrangian description on the troposphere-to-stratosphere transport changes associated with the stratospheric water drop around the year 2000, Atmospheric Chemistry and Physics, 16, 4235 4249, https://doi.org/10.5194/acp-16-4235-2016, cited by: 5; All Open Access, Gold Open Access, Green Open Access, 2016.

- Haynes, P. and Anglade, J.: The vertical-scale cascade in atmospheric tracers due to large-scale differential advection, Journal of the Atmospheric Sciences, 54, 1121 1136, https://doi.org/10.1175/1520-0469(1997)054<1121:TVSCIA>2.0.CO;2, cited by: 125; All Open Access, Bronze Open Access, 1997.
- Hersbach, H., Bell, B., Berrisford, P., Hirahara, S., Horányi, A., Muñoz-Sabater, J., Nicolas, J., Peubey, C., Radu, R., Schepers, D., Simmons, A., Soci, C., Abdalla, S., Abellan, X., Balsamo, G., Bechtold, P., Biavati, G., Bidlot, J., Bonavita, M., De Chiara, G., Dahlgren, P., Dee, D., Diamantakis, M., Dragani, R., Flemming, J., Forbes, R., Fuentes, M., Geer, A., Haimberger, L., Healy, S., Hogan, R. J., Hólm, E., Janisková, M., Keeley, S., Laloyaux, P., Lopez, P., Lupu, C., Radnoti, G., de Rosnay, P., Rozum, I., Vamborg, F., Villaume, S., and Thépaut, J.-N.: The ERA5 global reanalysis, Quarterly Journal of the Royal Meteorological Society, 146, 1999 2049, https://doi.org/10.1002/qj.3803, cited by: 11844; All Open Access, Hybrid Gold Open Access, 2020.
 - Holton, J. R. and Gettelman, A.: Horizontal transport and the dehydration of the stratosphere, Geophysical Research Letters, 28, 2799 2802, https://doi.org/10.1029/2001GL013148, cited by: 318, 2001.
 - Homeyer, C. R., Smith, J. B., Bedka, K. M., Bowman, K. P., Wilmouth, D. M., Ueyama, R., Dean-Day, J. M., St. Clair, J. M., Hannun, R., Hare, J., et al.: Extreme altitudes of stratospheric hydration by midlatitude convection observed during the DCOTSS field campaign, Geophysical Research Letters, 50, e2023GL104 914, 2023.

890

895

- Homeyer, C. R., Gordon, A. E., Smith, J. B., Ueyama, R., Wilmouth, D. M., Sayres, D. S., Hare, J., Pandey, A., Hanisco, T. F., Dean-Day, J. M., et al.: Stratospheric hydration processes in tropopause-overshooting convection revealed by tracer-tracer correlations from the DCOTSS field campaign, Journal of Geophysical Research: Atmospheres, 129, e2024JD041 340, 2024.
- Honomichl, S. B. and Pan, L. L.: Transport From the Asian Summer Monsoon Anticyclone Over the Western Pacific, Journal of Geophysical Research: Atmospheres, 125, https://doi.org/10.1029/2019JD032094, cited by: 27, 2020.
- James, R., Bonazzola, M., Legras, B., Surbled, K., and Fueglistaler, S. A.: Water vapor transport and dehydration above convective outflow during Asian monsoon, Geophysical Research Letters, 35, https://doi.org/10.1029/2008GL035441, cited by: 94; All Open Access; Bronze Open Access, 2008.
- Jensen, E., Pan, L., Honomichl, S., Diskin, G., Krämer, M., Spelten, N., Günther, G., Hurst, D., Fujiwara, M., Vömel, H., Selkirk, H., Suzuki, J., Schwartz, M., and Smith, J.: Assessment of Observational Evidence for Direct Convective Hydration of the Lower Stratosphere, Journal of Geophysical Research: Atmospheres, 125, https://doi.org/10.1029/2020JD032793, cited By 20, 2020.
- Jorgensen, D. and Lemone, M.: Vertical velocity characteristics of oceanic convection, Journal of the Atmospheric Sciences, 46, 621 640, https://doi.org/10.1175/1520-0469(1989)046<0621:VVCOOC>2.0.CO;2, cited by: 201; All Open Access, Bronze Open Access, 1989.
- Konopka, P., Tao, M., Von Hobe, M., Hoffmann, L., Kloss, C., Ravegnani, F., Volk, C. M., Lauther, V., Zahn, A., Hoor, P., and Ploeger, F.: Tropospheric transport and unresolved convection: numerical experiments with CLaMS 2.0/MESSy, Geoscientific Model Development, 15, 7471 7487, https://doi.org/10.5194/gmd-15-7471-2022, cited by: 5; All Open Access, Gold Open Access, Green Open Access, 2022.
- Konopka, P., Rolf, C., Von Hobe, M., Khaykin, S. M., Clouser, B., Moyer, E., Ravegnani, F., D'Amato, F., Viciani, S., Spelten, N., Afchine, A., Krämer, M., Stroh, F., and Ploeger, F.: The dehydration carousel of stratospheric water vapor in the Asian summer monsoon anticyclone, Atmospheric Chemistry and Physics, 23, 12 935 12 947, https://doi.org/10.5194/acp-23-12935-2023, 2023.
- 905 Kumar, V. and Krishnan, R.: On the association between the Indian summer monsoon and the tropical cyclone activity over northwest Pacific,

 Current science, pp. 602–612, 2005.
 - Lambert, A., Werner, F., Read, W. G., Froidevaux, L., Schwartz, M. J., Wagner, P. A., Daffer, W. H., Livesey, N. J., Pumphrey, H. C., Manney, G. L., et al.: Version 5 Level-2 Near-Real-Time Data User Guide, Tech. rep., Tech. Rep. JPL D-48439 d, Jet Propulsion Laboratory, California Institute of ..., 2017.

- 910 Liu, C., Zipser, E. J., and Nesbitt, S. W.: Global distribution of tropical deep convection: Different perspectives from TRMM infrared and radar data, Journal of Climate, 20, 489 503, https://doi.org/10.1175/JCLI4023.1, cited by: 190; All Open Access, Bronze Open Access, Green Open Access, 2007.
 - Liu, Y., Fueglistaler, S., and Haynes, P.: Advection-condensation paradigm for stratospheric water vapor, Journal of Geophysical Research Atmospheres, 115, https://doi.org/10.1029/2010JD014352, cited by: 62, 2010.
- Livesey, N., Read, W., Wagner, L., Froidevaux, P., Lambert, A., Manney, G., Millán Valle, L., Pumphrey, H., Santee, M., Schwartz, M., et al.: Version 4.2 x Level 2 and 3 data quality and description document (Tech. Rep. No. JPL D-33509 Rev. E), Jet Propulsion Laboratory, 2020.
 - McKenna, D. S., Grooß, J.-U., Günther, G., Konopka, P., Müller, R., Carver, G., and Sasano, Y.: A new Chemical Lagrangian Model of the Stratosphere (CLaMS) 2. Formulation of chemistry scheme and initialization, Journal of Geophysical Research Atmospheres, 107, ACH 4–1 ACH 4–14, https://doi.org/10.1029/2000JD000113, cited by: 116, 2002.
- 920 Mote, P. W., Rosenlof, K. H., Holton, J. R., Harwood, R. S., and Waters, J. W.: Seasonal variations of water vapor in the tropical lower stratosphere, Geophysical Research Letters, 22, 1093 1096, https://doi.org/10.1029/95GL01234, cited by: 83, 1995.

- Mote, P. W., Rosenlof, K. H., McIntyre, M. E., Carr, E. S., Gille, J. C., Holton, J. R., Kinnersley, J. S., Pumphrey, H. C., Russell III, J. M., and Waters, J. W.: An atmospheric tape recorder: The imprint of tropical tropopause temperatures on stratospheric water vapor, Journal of Geophysical Research Atmospheres, 101, 3989 4006, https://doi.org/10.1029/95JD03422, cited by: 626; All Open Access, Green Open Access, 1996.
- Nützel, M., Podglajen, A., Garny, H., and Ploeger, F.: Quantification of water vapour transport from the Asian monsoon to the stratosphere, Atmospheric Chemistry and Physics, 19, 8947 8966, https://doi.org/10.5194/acp-19-8947-2019, cited by: 22; All Open Access, Gold Open Access, 2019.
- O'Neill, M., Orf, L., Heymsfield, G., and Halbert, K.: Hydraulic jump dynamics above supercell thunderstorms, Science, 373, 1248–1251, https://doi.org/10.1126/science.abh3857, cited By 24, 2021.
 - Park, M., Randel, W. J., Gettelman, A., Massie, S. T., and Jiang, J. H.: Transport above the Asian summer monsoon anticyclone inferred from Aura Microwave Limb Sounder tracers, Journal of Geophysical Research Atmospheres, 112, https://doi.org/10.1029/2006JD008294, cited by: 280; All Open Access, Bronze Open Access, Green Open Access, 2007.
- Park, M., Randel, W. J., Damadeo, R. P., Flittner, D. E., Davis, S. M., Rosenlof, K. H., Livesey, N., Lambert, A., and Read, W.: Near-935 Global Variability of Stratospheric Water Vapor Observed by SAGE III/ISS, Journal of Geophysical Research: Atmospheres, 126, https://doi.org/10.1029/2020JD034274, cited by: 6; All Open Access, Green Open Access, 2021.
 - Peña-Ortiz, C., Plaza, N. P., Gallego, D., and Ploeger, F.: Quasi-biennial oscillation modulation of stratospheric water vapour in the Asian monsoon, Atmospheric Chemistry and Physics, 24, 5457 5478, https://doi.org/10.5194/acp-24-5457-2024, cited by: 0, 2024.
- Pierrehumbert, R. T. and Roca, R.: Evidence for control of atlantic subtropical humidity by large scale advection, Geophysical Research

 Letters, 25, 4537 4540, https://doi.org/10.1029/1998GL900203, cited by: 114; All Open Access; Green Accepted Open Access; Green

 Open Access, 1998.
 - Pisso, I., Marécal, V., Legras, B., and Berthet, G.: Sensitivity of ensemble Lagrangian reconstructions to assimilated wind time step resolution, Atmospheric Chemistry and Physics, 10, 3155–3162, https://doi.org/10.5194/acp-10-3155-2010, cited By 11, 2010.
- Plaza, N. P., Podglajen, A., Peña-Ortiz, C., and Ploeger, F.: Processes influencing lower stratospheric water vapour in monsoon anticyclones: insights from Lagrangian modelling, Atmospheric Chemistry and Physics, 21, 9585–9607, 2021.

- Ploeger, F., Fueglistaler, S., Grooß, J.-U., Günther, G., Konopka, P., Liu, Y., Uller, R., Ravegnani, F., Schiller, C., Ulanovski, A., and Riese, M.: Insight from ozone and water vapour on transport in the tropical tropopause layer (TTL), Atmospheric Chemistry and Physics, 11, 407–419, https://doi.org/10.5194/acp-11-407-2011, cited By 54, 2011.
- Ploeger, F., Günther, G., Konopka, P., Fueglistaler, S., Müller, R., Hoppe, C., Kunz, A., Spang, R., Grooß, J.-U., and Riese, M.: Horizontal water vapor transport in the lower stratosphere from subtropics to high latitudes during boreal summer, Journal of Geophysical Research Atmospheres, 118, 8111 8127, https://doi.org/10.1002/jgrd.50636, cited by: 98; All Open Access, Green Open Access, 2013.
 - Poshyvailo, L., Müller, R., Konopka, P., Günther, G., Riese, M., Podglajen, A., and Ploeger, F.: Sensitivities of modelled water vapour in the lower stratosphere: Temperature uncertainty, effects of horizontal transport and small-scale mixing, Atmospheric Chemistry and Physics, 18, 8505–8527, https://doi.org/10.5194/acp-18-8505-2018, cited By 18, 2018.
- 955 Randel, W. and Park, M.: Diagnosing Observed Stratospheric Water Vapor Relationships to the Cold Point Tropical Tropopause, Journal of Geophysical Research: Atmospheres, 124, 7018–7033, https://doi.org/10.1029/2019JD030648, cited By 50, 2019.
 - Randel, W., Moyer, E., Park, M., Jensen, E., Bernath, P., Walker, K., and Boone, C.: Global variations of HDO and HDO/H2O ratios in the upper troposphere and lower stratosphere derived from ACE-FTS satellite measurements, Journal of Geophysical Research Atmospheres, 117, https://doi.org/10.1029/2011JD016632, cited By 69, 2012.
- 960 Randel, W. J., Wu, F., Oltmans, S. J., Rosenlof, K., and Nedoluha, G. E.: Interannual changes of stratospheric water vapor and correlations with tropical tropopause temperatures, Journal of the Atmospheric Sciences, 61, 2133 2148, , cited by: 216; All Open Access, Bronze Open Access, 2004.
 - Randel, W. J., Zhang, K., and Fu, R.: What controls stratospheric water vapor in the NH summer monsoon regions?, JOURNAL OF GEO-PHYSICAL RESEARCH-ATMOSPHERES, 120, 7988–8001, https://doi.org/10.1002/2015JD023622, 2015.
- Read, W., Lambert, A., Bacmeister, J., Cofield, R., Christensen, L., Cuddy, D., Daffer, W., Drouin, B., Fetzer, E., Froidevaux, L., Fuller, R., Herman, R., Jarnot, R., Jiang, J., Jiang, Y., Kelly, K., Knosp, B., Kovalenko, L., Livesey, N., Liu, H.-C., Manney, G., Pickett, H., Pumphrey, H., Rosenlof, K. H., Sabounchi, X., Santee, M., Schwartz, M., Snyder, W., Stek, P., Su, H., Takacs, L., Thurstans, R., Vömel, H., Wagner, P., Waters, J., Webster, C., Weinstock, E., and Wu, D.: Aura Microwave Limb Sounder upper tropospheric and lower stratospheric H2O and relative humidity with respect to ice validation, Journal of Geophysical Research Atmospheres, 112, https://doi.org/10.1029/2007JD008752, cited by: 193; All Open Access, Bronze Open Access, 2007.
 - Riese, M., Ploeger, F., Rap, A., Vogel, B., Konopka, P., Dameris, M., and Forster, P.: Impact of uncertainties in atmospheric mixing on simulated UTLS composition and related radiative effects, JOURNAL OF GEOPHYSICAL RESEARCH-ATMOSPHERES, 117, https://doi.org/10.1029/2012JD017751, 2012.
- Rolf, C., Vogel, B., Hoor, P., Afchine, A., Günther, G., Krämer, M., Müller, R., Müller, S., Spelten, N., and Riese, M.: Water vapor increase in the lower stratosphere of the Northern Hemisphere due to the Asian monsoon anticyclone observed during the TACTS/ESMVal campaigns, Atmospheric Chemistry and Physics, 18, 2973 2983, cited by: 23; All Open Access, Gold Open Access, 2018.
 - Schiller, C., Groob, J.-U., Konopka, P., Plöger, F., Silva Dos Santos, F., and Spelten, N.: Hydration and dehydration at the tropical tropopause, Atmospheric Chemistry and Physics, 9, 9647–9660, https://doi.org/10.5194/acp-9-9647-2009, cited By 73, 2009.
- Schoeberl, M. and Dessler, A.: Dehydration of the stratosphere, Atmospheric Chemistry and Physics, 11, 8433 8446, 980 https://doi.org/10.5194/acp-11-8433-2011, cited by: 92; All Open Access, Gold Open Access, Green Open Access, 2011.
 - Schoeberl, M. R., Dessler, A. E., and Wang, T.: Modeling upper tropospheric and lower stratospheric water vapor anomalies, Atmospheric Chemistry and Physics, 13, 7783–7793, , 2013.

- Schwartz, M. J., Read, W. G., Santee, M. L., Livesey, N. J., Froidevaux, L., Lambert, A., and Manney, G. L.: Convectively injected water vapor in the North American summer lowermost stratosphere, Geophysical Research Letters, 40, 2316 2321, https://doi.org/10.1002/grl.50421, cited by: 70; All Open Access, Bronze Open Access, 2013.
 - Smith, J., Wilmouth, D., Bedka, K., Bowman, K., Homeyer, C., Dykema, J., Sargent, M., Clapp, C., Leroy, S., Sayres, D., Dean-Day, J., Paul Bui, T., and Anderson, J.: A case study of convectively sourced water vapor observed in the overworld stratosphere over the United States, Journal of Geophysical Research: Atmospheres, 122, 9529–9554, https://doi.org/10.1002/2017JD026831, cited By 64, 2017.
- Smith, J., Haynes, P., Maycock, A., Butchart, N., and Bushell, A.: Sensitivity of stratospheric water vapour to variability in tropical tropopause temperatures and large-scale transport, Atmospheric Chemistry and Physics, 21, 2469–2489, https://doi.org/10.5194/acp-21-2469-2021, cited By 7, 2021.
 - Solomon, S., Rosenlof, K. H., Portmann, R. W., Daniel, J. S., Davis, S. M., Sanford, T. J., and Plattner, G.-K.: Contributions of Stratospheric Water Vapor to Decadal Changes in the Rate of Global Warming, SCIENCE, 327, 1219–1223, https://doi.org/10.1126/science.1182488, 2010.
- Sonntag, D.: Advancements in the field of hygrometry, Meteorologische Zeitschrift, 3, 51–66, https://doi.org/10.1127/metz/3/1994/51, 1994.

 Tao, M., Konopka, P., Wright, J. S., Liu, Y., Bian, J., Davis, S. M., Jia, Y., and Ploeger, F.: Multi-decadal variability controls short-term stratospheric water vapor trends, Communications Earth and Environment, 4, , cited by: 2; All Open Access, Gold Open Access, 2023.

- Ueyama, R., Jensen, E., Pfister, L., Krämer, M., Afchine, A., and Schoeberl, M.: Impact of Convectively Detrained Ice Crystals on the Humidity of the Tropical Tropopause Layer in Boreal Winter, Journal of Geophysical Research: Atmospheres, 125, https://doi.org/10.1029/2020JD032894, cited By 9, 2020.
- Ueyama, R., Schoeberl, M., Jensen, E., Pfister, L., Park, M., and Ryoo, J.-M.: Convective Impact on the Global Lower Stratospheric Water Vapor Budget, Journal of Geophysical Research: Atmospheres, 128, https://doi.org/10.1029/2022JD037135, cited By 8, 2023.
- Uma, K. N., Das, S. K., and Das, S. S.: A climatological perspective of water vapor at the UTLS region over different global monsoon regions: Observations inferred from the Aura-MLS and reanalysis data, Climate Dynamics, 43, 407 420, https://doi.org/10.1007/s00382-014-2085-9, cited by: 37, 2014.
- Vogel, B., Müller, R., Günther, G., Spang, R., Hanumanthu, S., Li, D., Riese, M., and Stiller, G.: Lagrangian simulations of the transport of young air masses to the top of the Asian monsoon anticyclone and into the tropical pipe, Atmospheric Chemistry and Physics, 19, 6007–6034, https://doi.org/10.5194/acp-19-6007-2019, cited By 64, 2019.
- Waters, J. W., Froidevaux, L., Harwood, R. S., Jarnot, R. F., Pickett, H. M., Read, W. G., Siegel, P. H., Cofield, R. E., Filipiak, M. J., Flower,
 D. A., et al.: The earth observing system microwave limb sounder (EOS MLS) on the Aura satellite, IEEE transactions on geoscience and remote sensing, 44, 1075–1092, 2006.
 - Wright, C. and Gille, J.: HIRDLS observations of gravity wave momentum fluxes over the monsoon regions, Journal of Geophysical Research Atmospheres, 116, , cited by: 35, 2011.
- Yu, W., Dessler, A. E., Park, M., and Jensen, E. J.: Influence of convection on stratospheric water vapor in the North American monsoon region, Atmospheric Chemistry and Physics, 20, 12153 12161, https://doi.org/10.5194/acp-20-12153-2020, cited by: 12; All Open Access, Gold Open Access, Green Open Access, 2020.